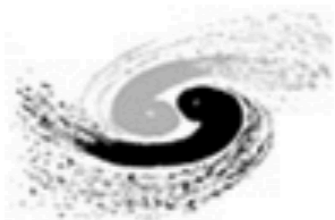




Neutralino DM Search in ATLAS

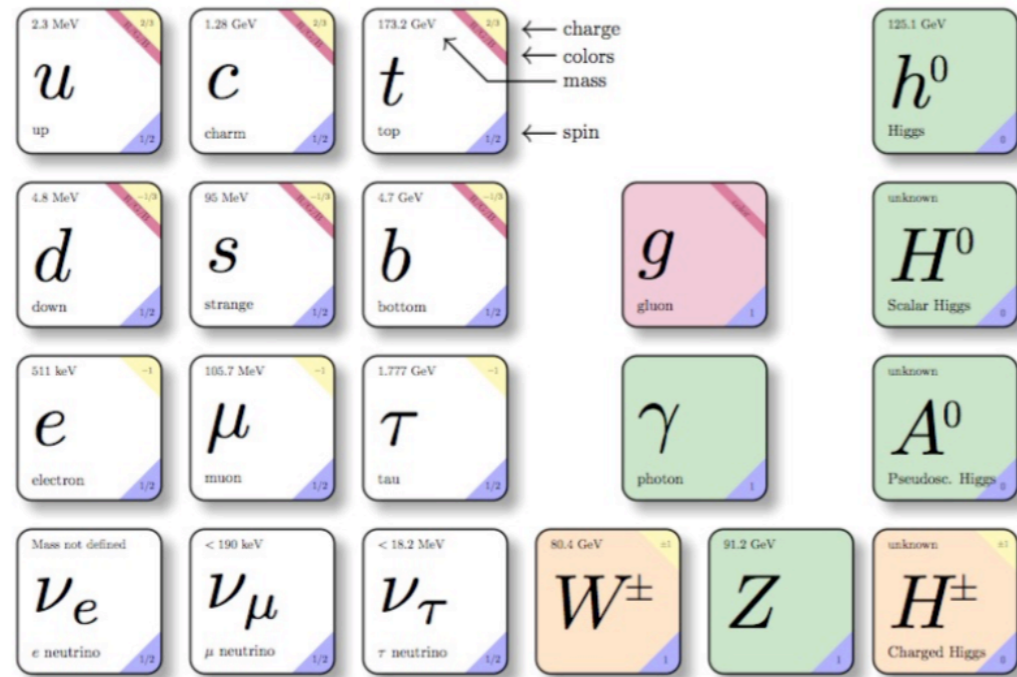
Da XU (IHEP, CAS)
COUSP 2024



中国科学院高能物理研究所
Institute of High Energy Physics Chinese Academy of Sciences

Supersymmetry

Extended Standard Model particles



Supersymmetric particles

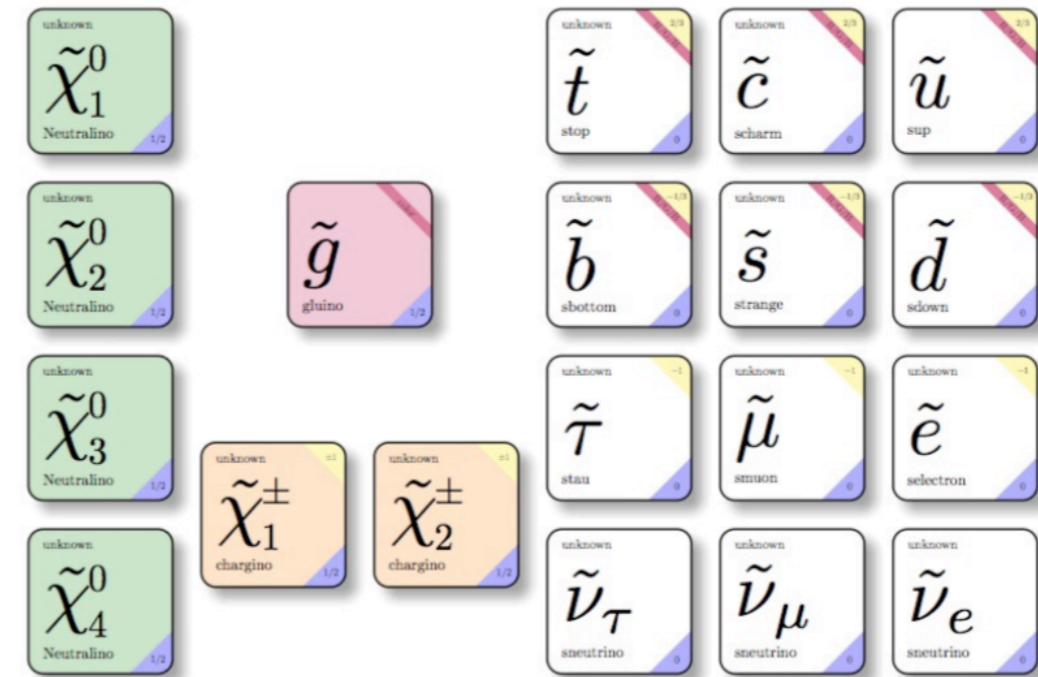
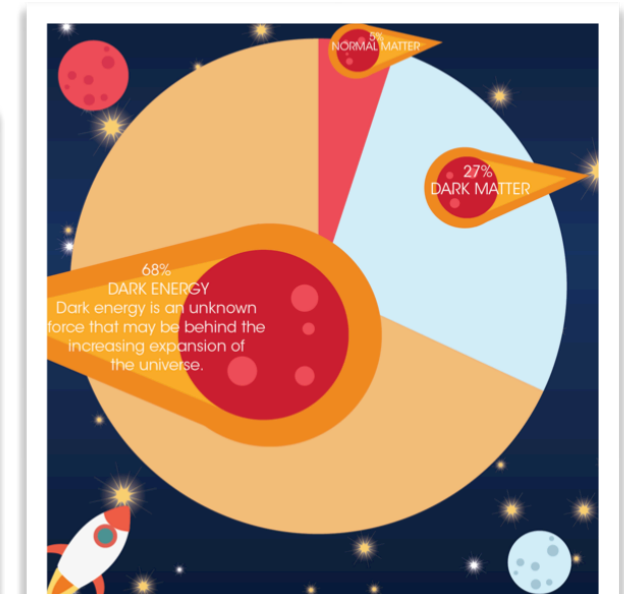
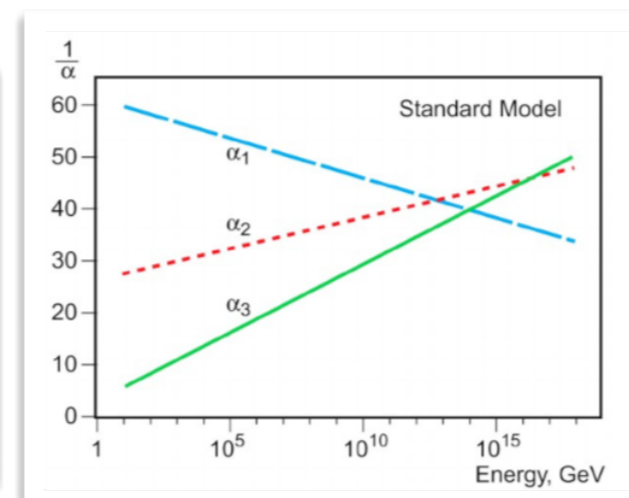
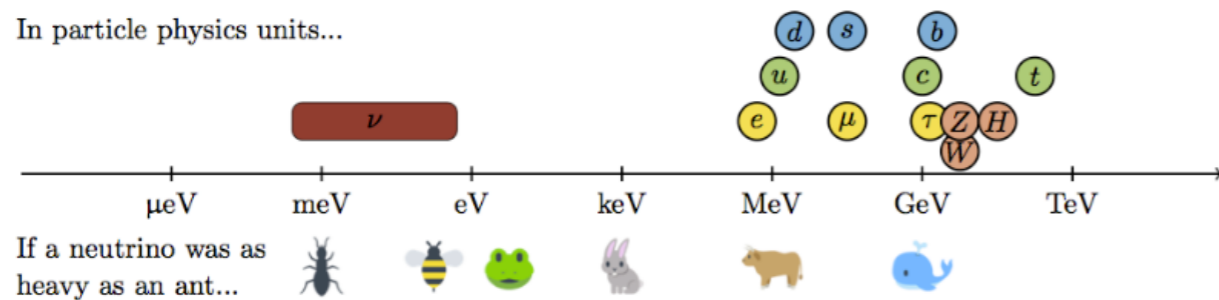


Image credit: M. Rimoldi

In particle physics units...



The Lightest Neutralino

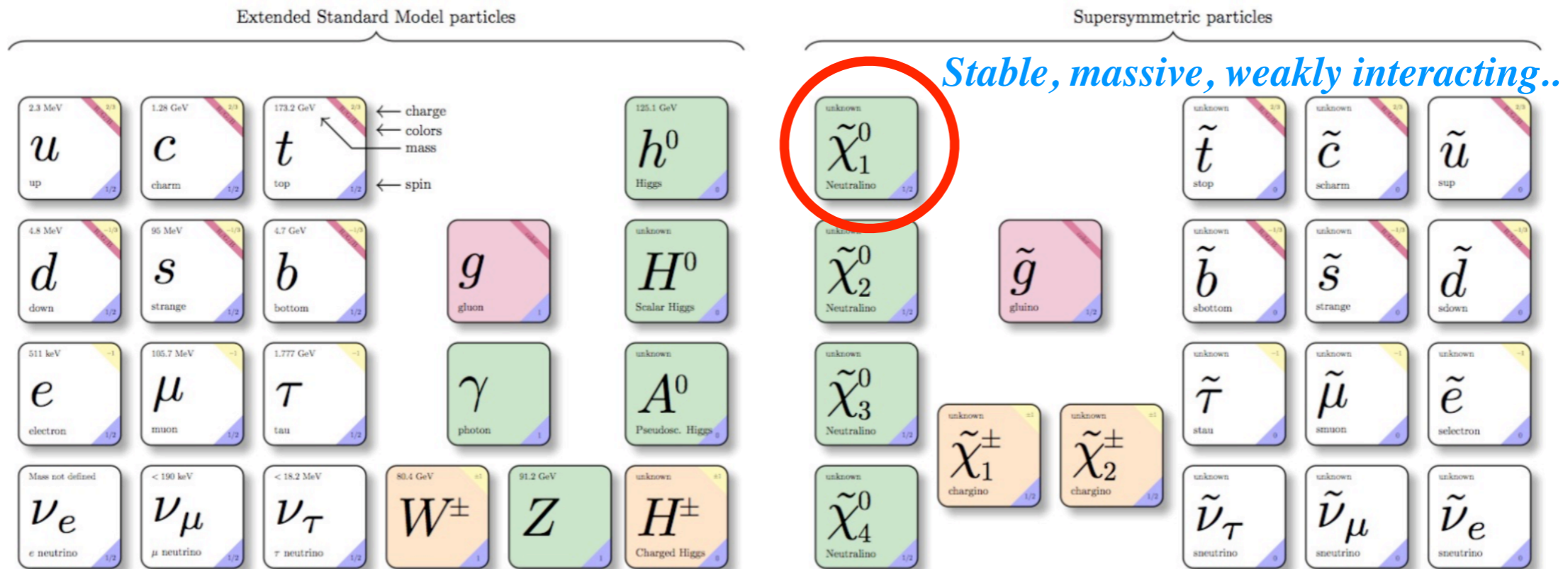
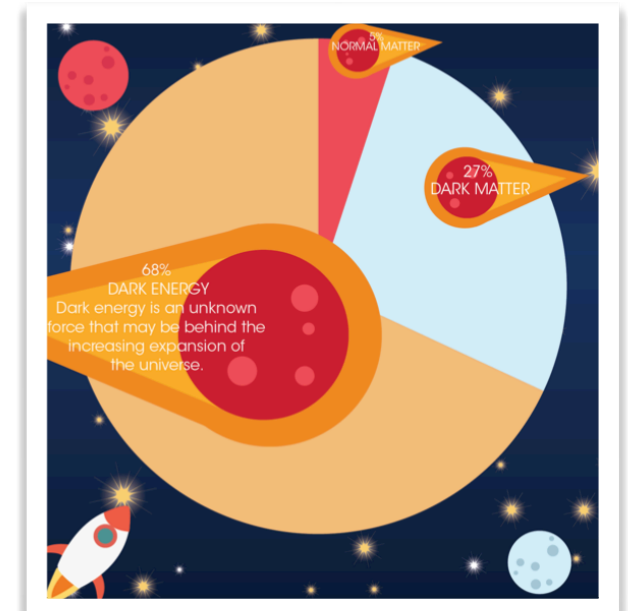
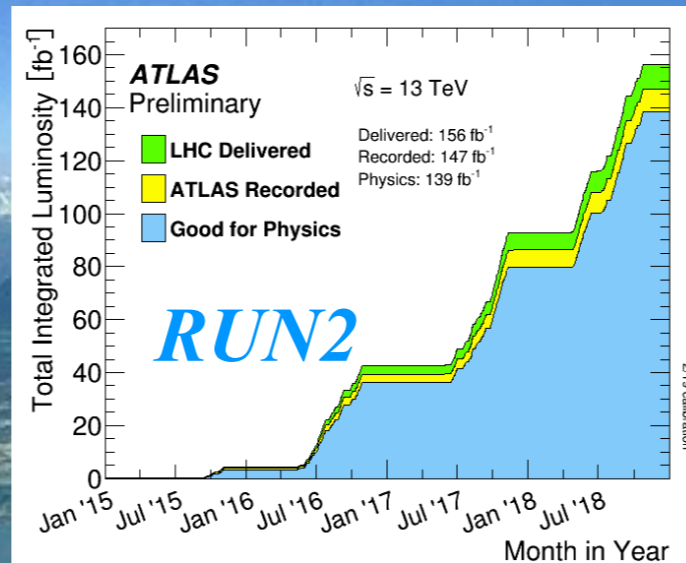


Image credit: M. Rimoldi

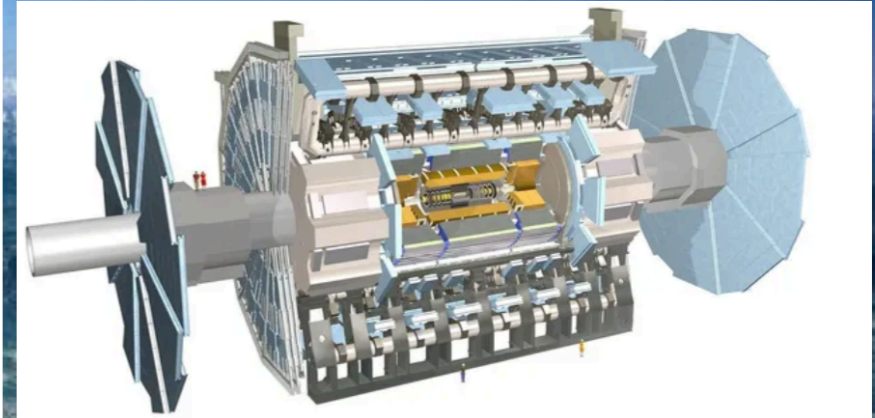
In R-parity conserving SUSY scenario, *the lightest neutralino as lightest supersymmetric particle (LSP) is one of the oldest and most studied examples of a WIMP candidate for the cosmological Dark Matter*



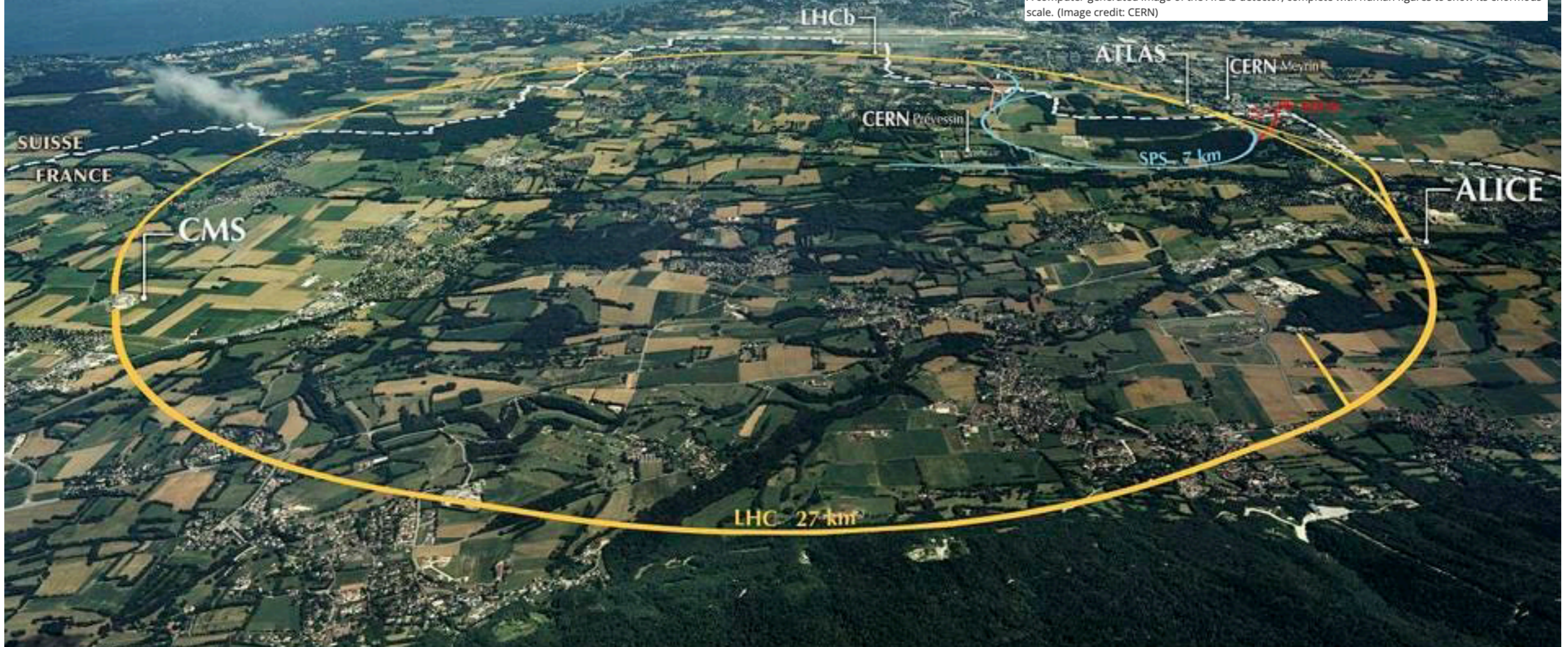
ATLAS in LHC



ATLAS detector



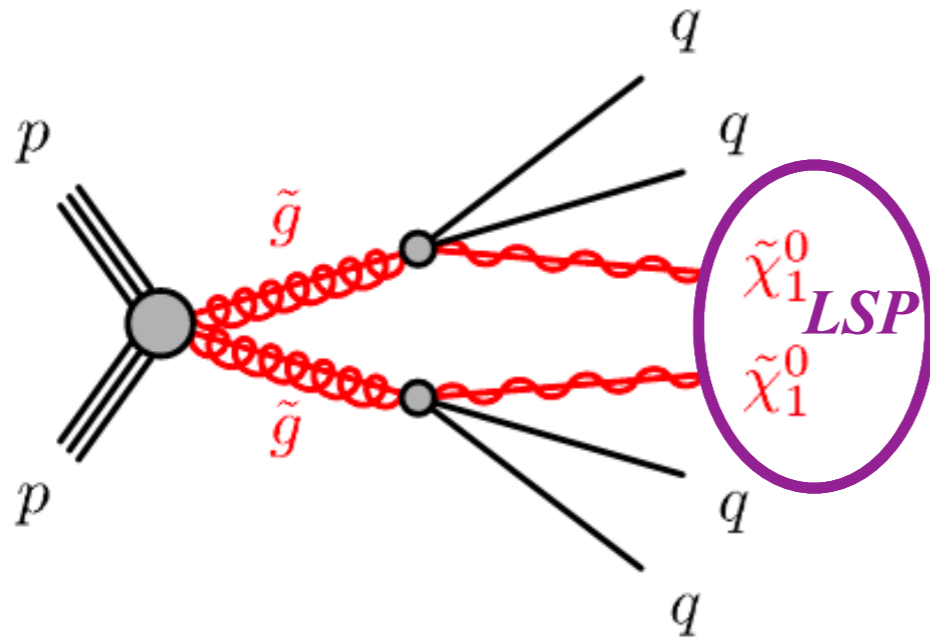
A computer-generated image of the ATLAS detector, complete with human figures to show its enormous scale. (Image credit: CERN)



Outline

- **Summary on ATLAS full Run2 *RPC* SUSY search (*Simplified model* based)**
- **Fresh re-interpretation from *pMSSM***
- **Outlook for HL-LHC**

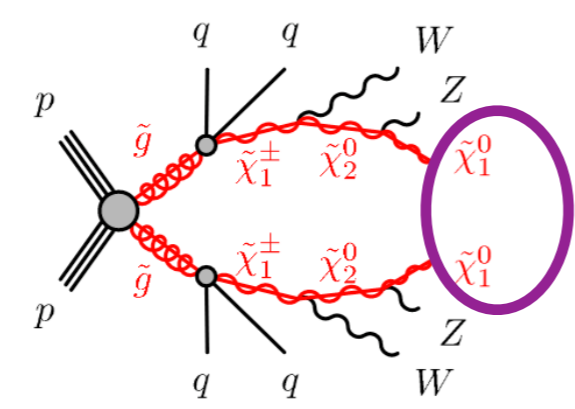
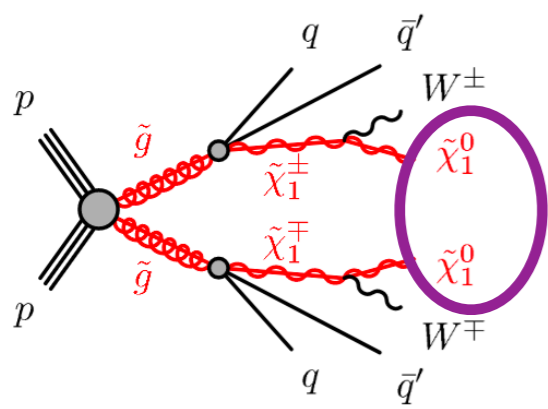
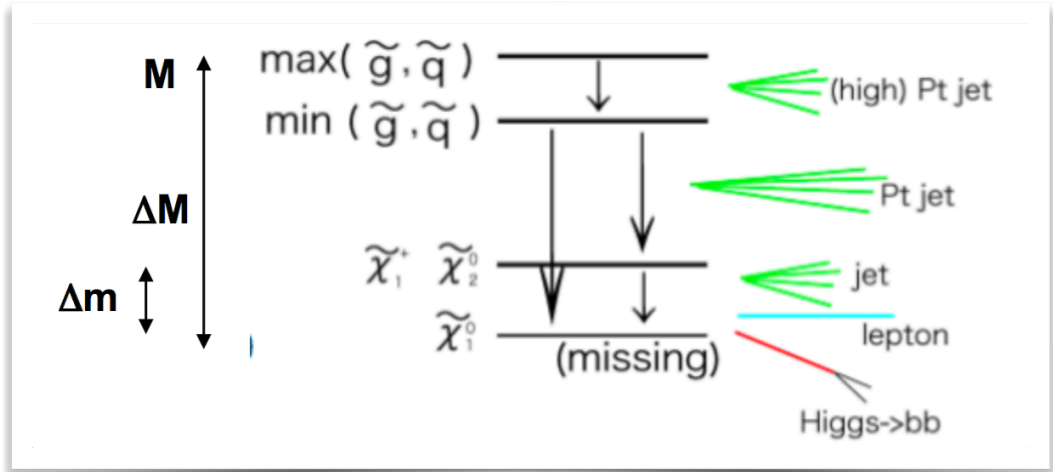
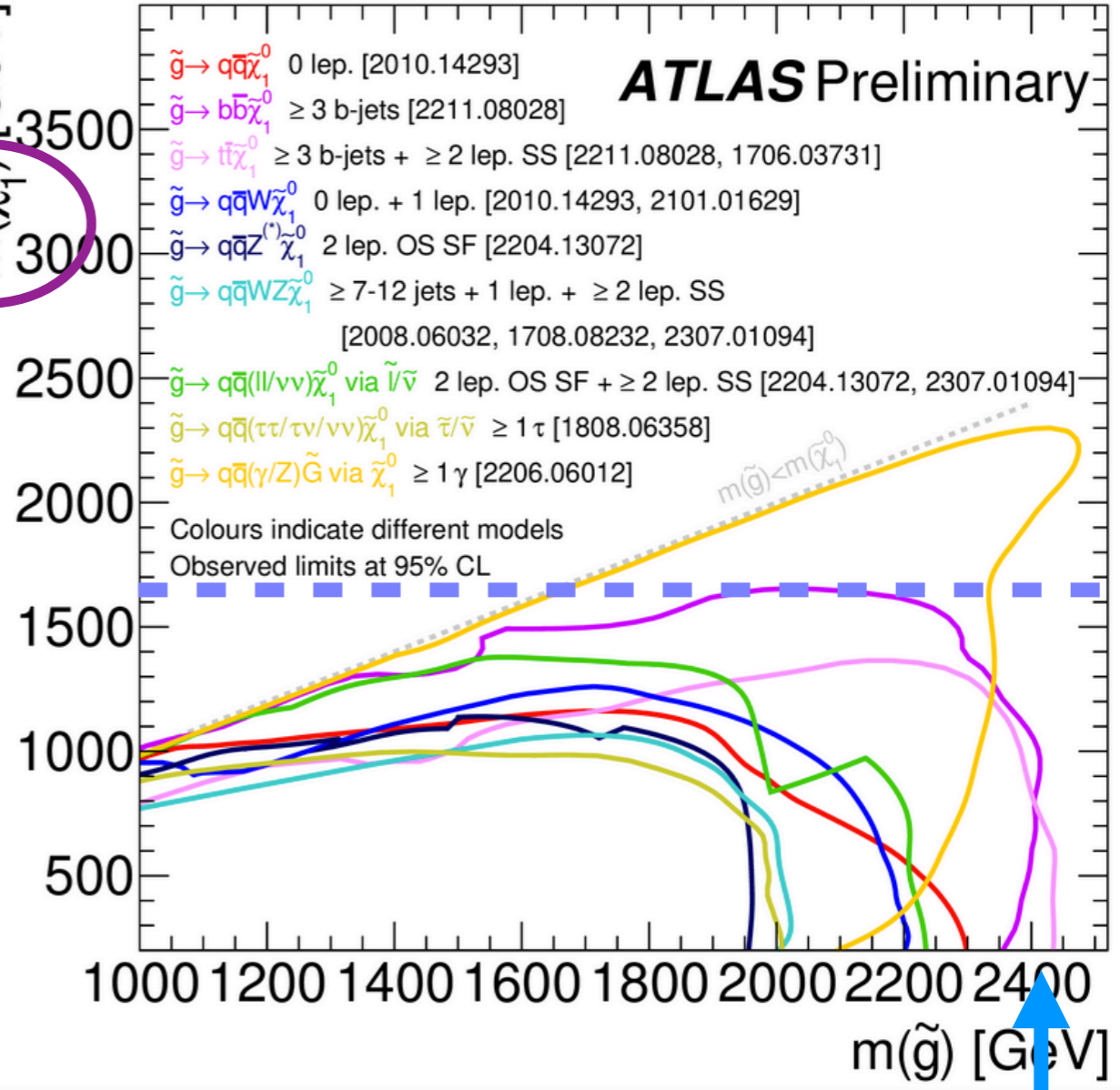
Constraint from gluino search



$m(\tilde{\chi}_1^0)$ [GeV]

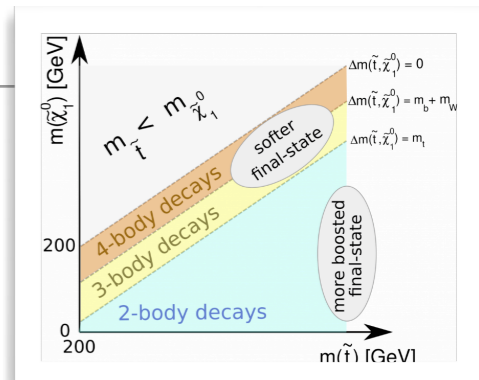
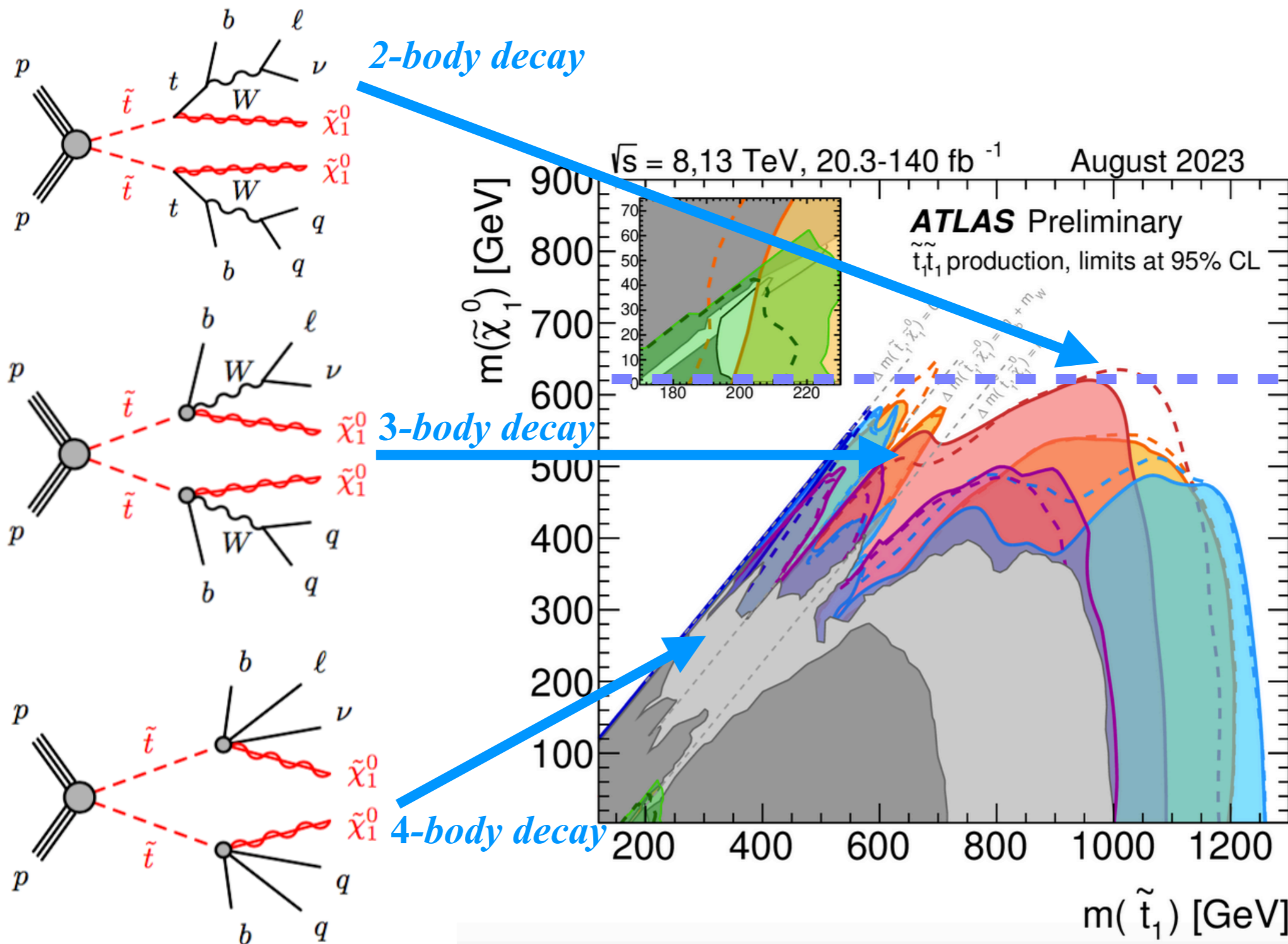
$\sqrt{s} = 13 \text{ TeV}, 36.1 - 140 \text{ fb}^{-1}$ March 2023

ATLAS Preliminary





Constraint from stop search



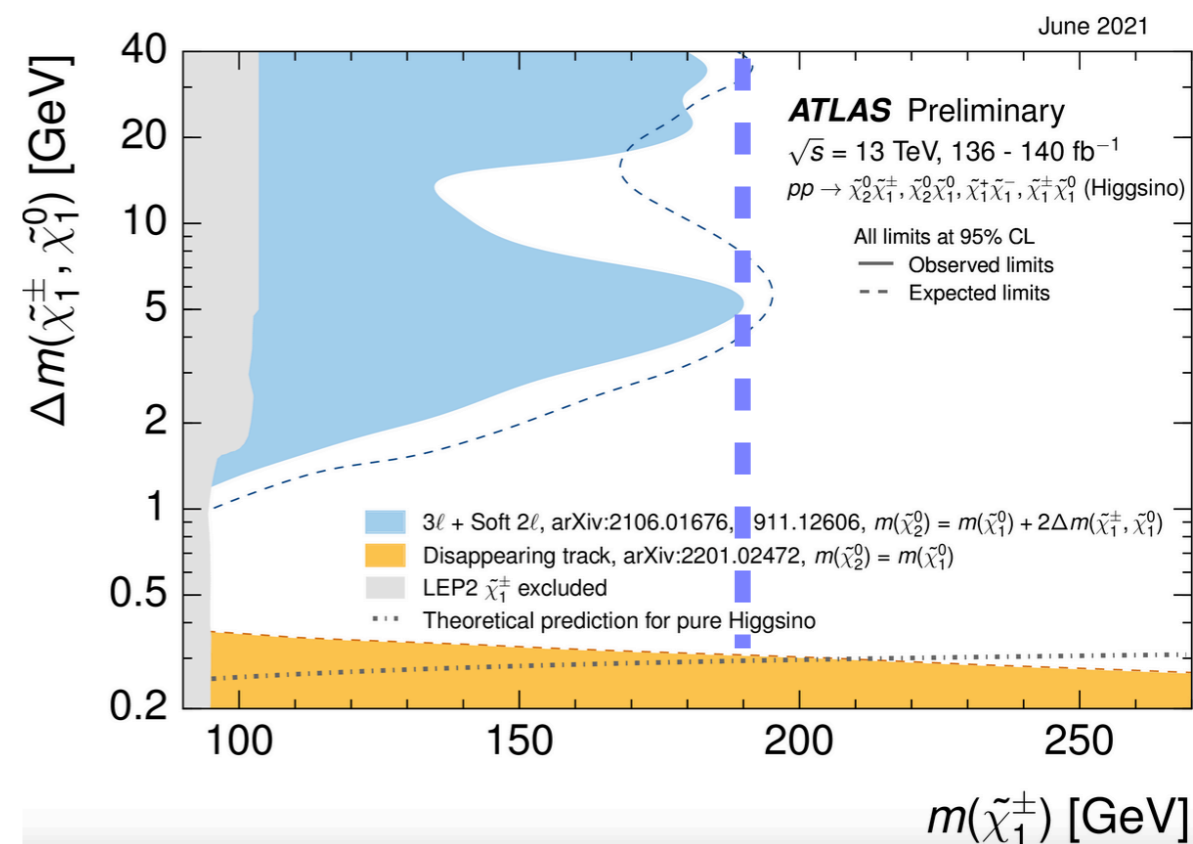
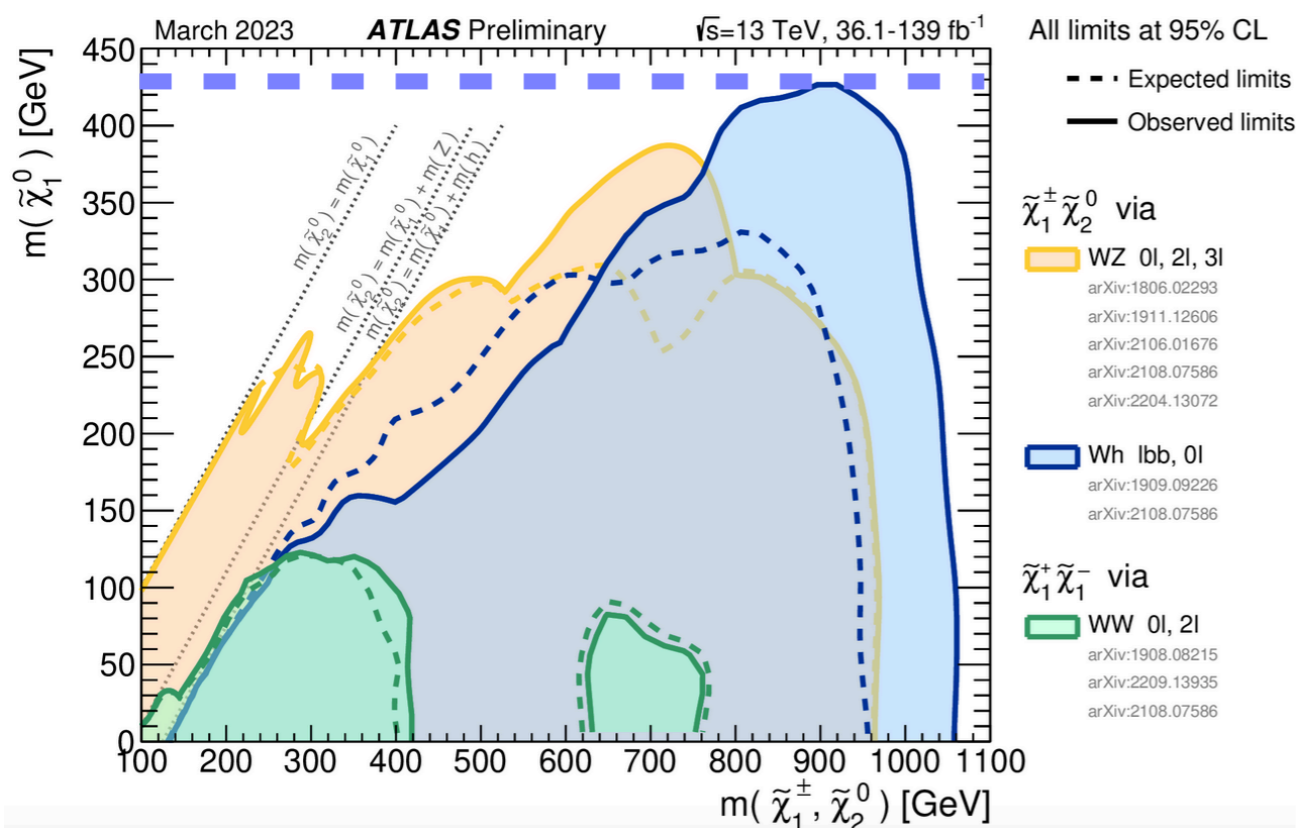
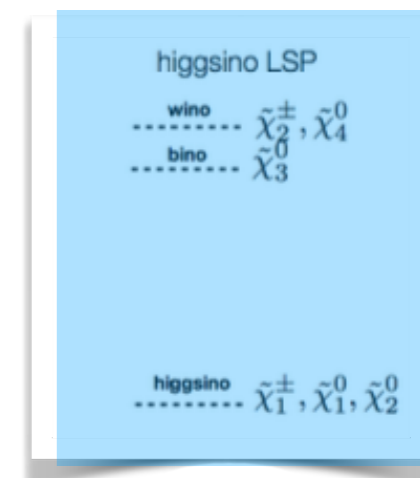
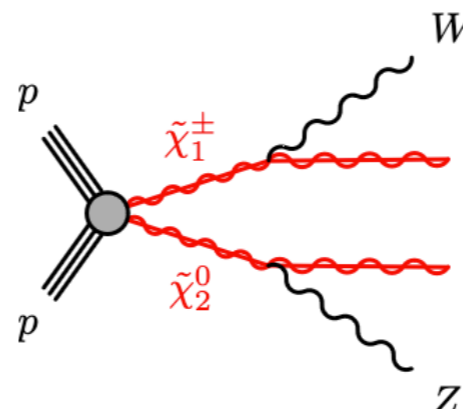
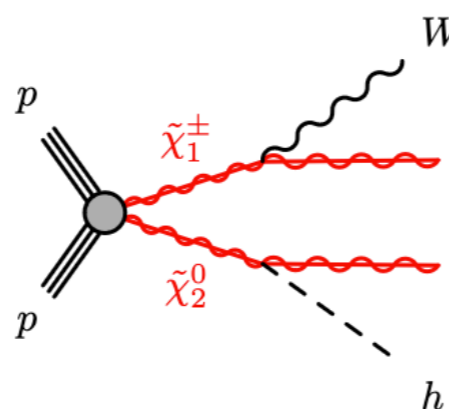
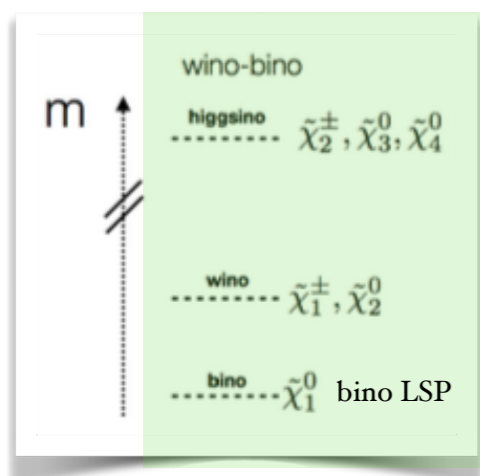
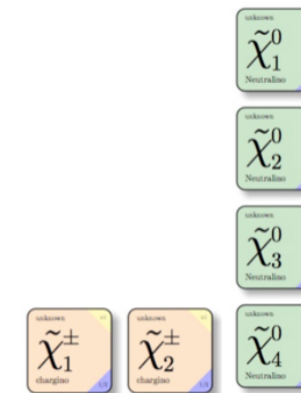
- Observed limits
- - - Expected limits

- Data 15-18, $\sqrt{s} = 13 \text{ TeV}, 140 \text{ fb}^{-1}$
- monojet, $\tilde{t}_1 \rightarrow bff \tilde{\chi}_1^0$ [2102.10874]
- 0L, $\tilde{t}_1 \rightarrow t\tilde{\chi}_1^0 / \tilde{t}_1 \rightarrow bW\tilde{\chi}_1^0 / \tilde{t}_1 \rightarrow bff \tilde{\chi}_1^0$ [2004.14060]
- 1L, $\tilde{t}_1 \rightarrow t\tilde{\chi}_1^0 / \tilde{t}_1 \rightarrow bW\tilde{\chi}_1^0 / \tilde{t}_1 \rightarrow bff \tilde{\chi}_1^0$ [2012.03799]
- 1L NN, $\tilde{t}_1 \rightarrow t\tilde{\chi}_1^0 / \tilde{t}_1 \rightarrow bW\tilde{\chi}_1^0$ [ATLAS-CONF-2023-043]
- 2L, $\tilde{t}_1 \rightarrow t\tilde{\chi}_1^0 / \tilde{t}_1 \rightarrow bW\tilde{\chi}_1^0 / \tilde{t}_1 \rightarrow bff \tilde{\chi}_1^0$ [2102.01444]

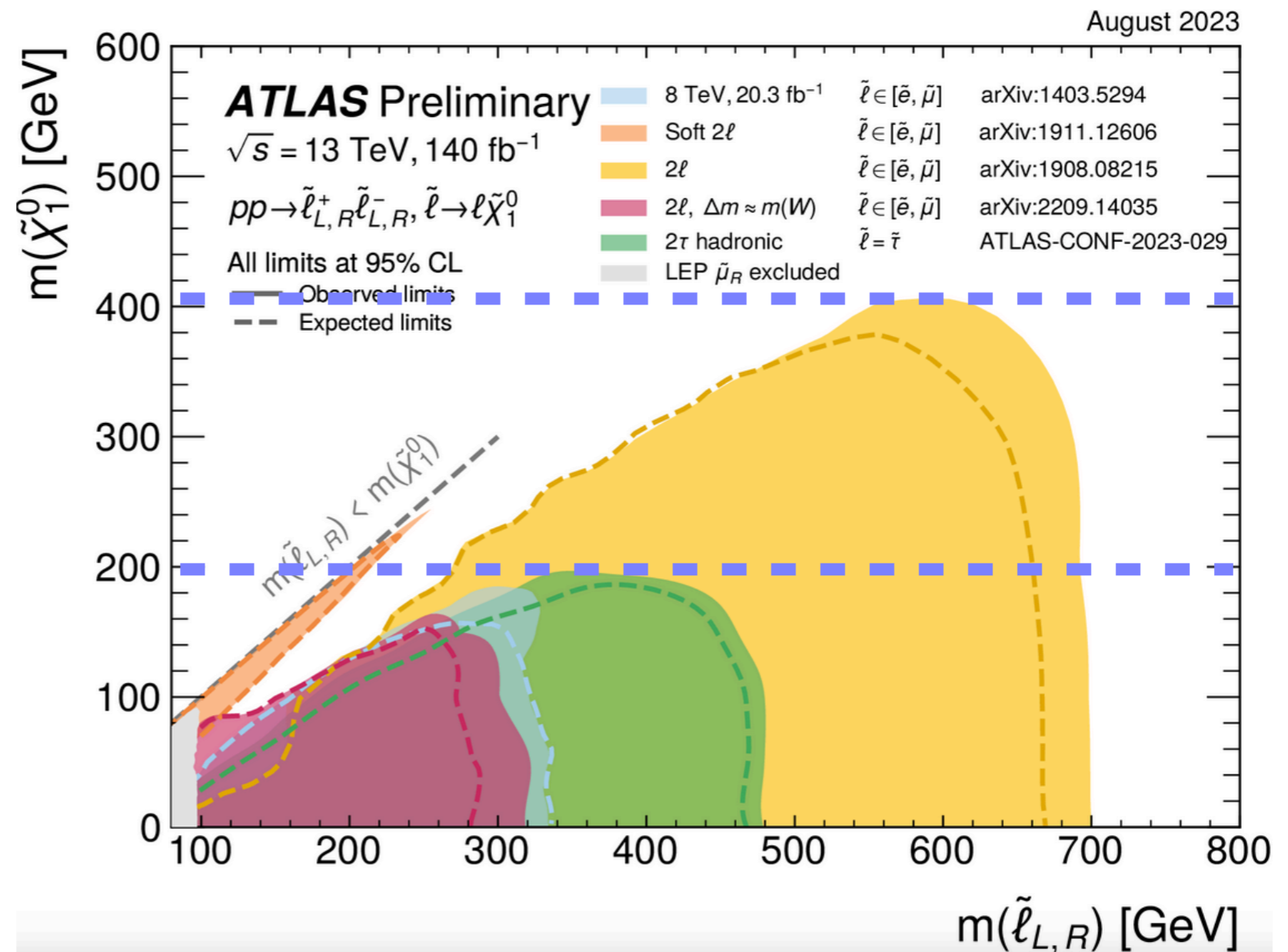
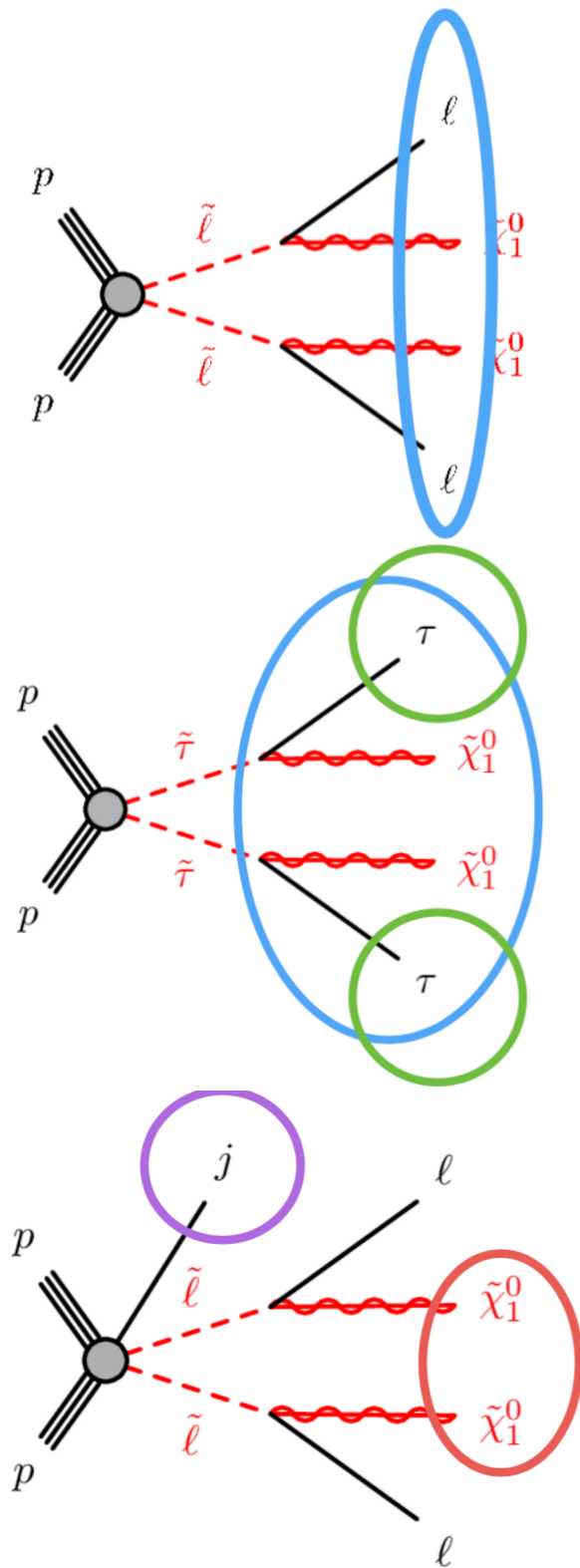
- Data 15-16, $\sqrt{s} = 13 \text{ TeV}, 36.1 \text{ fb}^{-1}$
- $\tilde{t}_1 \rightarrow t\tilde{\chi}_1^0 / \tilde{t}_1 \rightarrow bW\tilde{\chi}_1^0 / \tilde{t}_1 \rightarrow bff \tilde{\chi}_1^0$ [1709.04183, 1711.11520, 1708.03247, 1711.03301]
- $\tilde{t}, \tilde{t}_1 \rightarrow t\tilde{\chi}_1^0$ [1903.07570]

- Data 12, $\sqrt{s} = 8 \text{ TeV}, 20.3 \text{ fb}^{-1}$
- $\tilde{t}_1 \rightarrow t\tilde{\chi}_1^0 / \tilde{t}_1 \rightarrow bW\tilde{\chi}_1^0 / \tilde{t}_1 \rightarrow bff \tilde{\chi}_1^0$ [1506.08616]

Constraint from chargino/neutralino search



Constraint from direct slepton search



In Simplified Models, only the masses of relevant sparticles are free parameters.

We hope to project our results into a closer to reality model.

EWK pMSSM model

- **19 free parameters** \rightarrow i.e. $\sim 400k$ models for **BinoDM scan**

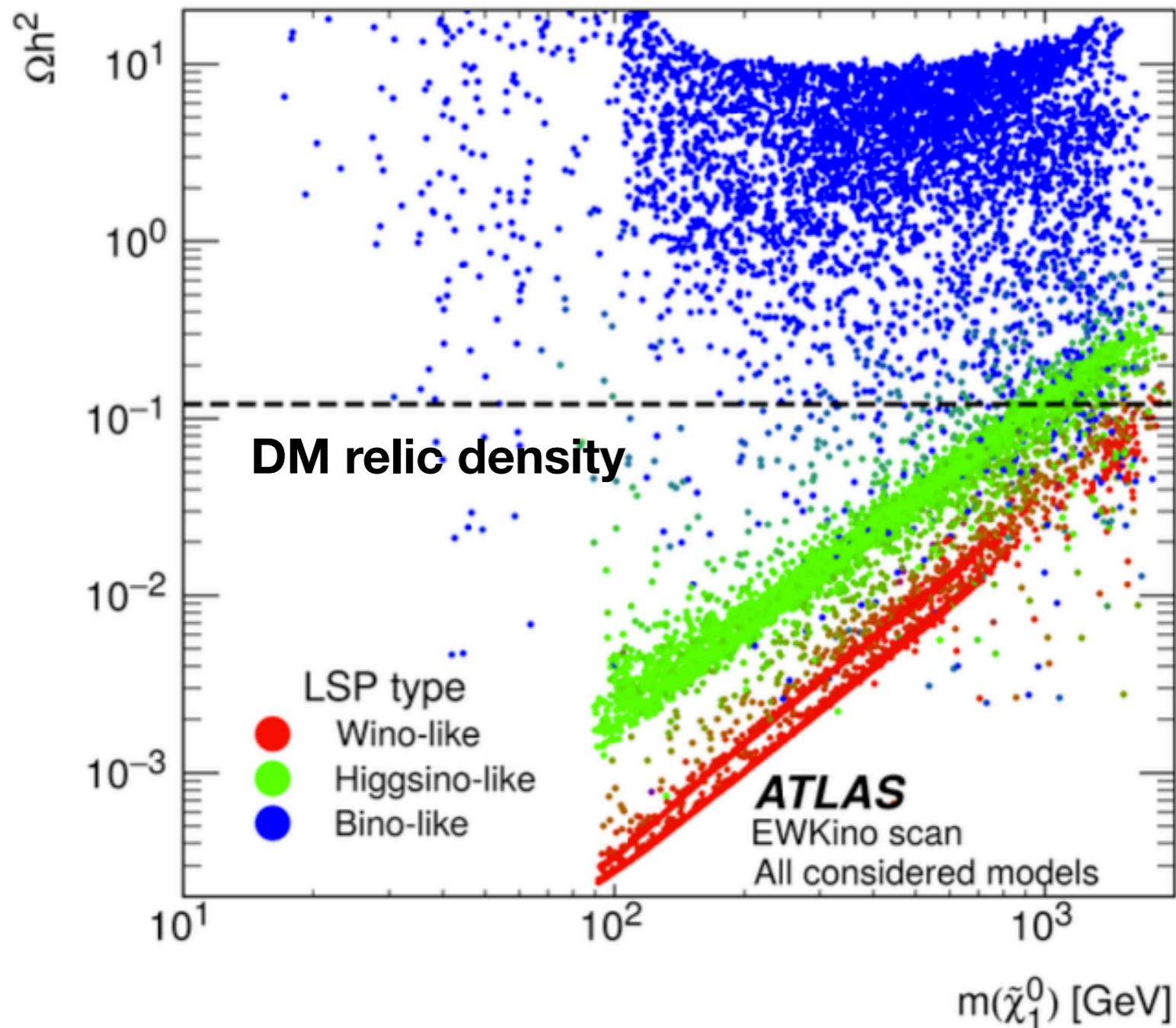
Parameter	Note
$M_{\tilde{L}_1}$ ($=M_{\tilde{L}_2}$)	Left-handed slepton (first two gens.) mass
$M_{\tilde{e}_1}$ ($=M_{\tilde{e}_2}$)	Right-handed slepton (first two gens.) mass
$M_{\tilde{L}_3}$	Left-handed stau doublet mass
$M_{\tilde{e}_3}$	Right-handed stau mass
$M_{\tilde{Q}_1}$ ($=M_{\tilde{Q}_2}$)	Left-handed squark (first two gens.) mass
$M_{\tilde{u}_1}$ ($=M_{\tilde{u}_2}$)	Right-handed up-type squark (first two gens.) mass
$M_{\tilde{d}_1}$ ($=M_{\tilde{d}_2}$)	Right-handed down-type squark (first two gens.) mass
$M_{\tilde{Q}_3}$	Left-handed squark (third gen.) mass
$M_{\tilde{u}_3}$	Right-handed top squark mass
$M_{\tilde{d}_3}$	Right-handed bottom squark mass
M_1	Bino mass parameter
M_2	Wino mass parameter
μ	Bilinear Higgs boson mass parameter
M_3	Gluino mass parameter
A_t	Trilinear top coupling
A_b	Trilinear bottom coupling
A_τ	Trilinear τ -lepton coupling
M_A	Pseudoscalar Higgs boson mass
$\tan\beta$	Ratio of the Higgs vacuum expectation values

Emphasis was on the electroweak sector, with the gluino, squarks, and sleptons having very high masses.

Analysis	Relevant simplified models targeted
FullHad [24]	Wino $\tilde{\chi}_1^\pm \tilde{\chi}_2^0$ via WZ, Wino $\tilde{\chi}_1^\pm \tilde{\chi}_2^0$ via Wh , Wino $\tilde{\chi}_1^+ \tilde{\chi}_1^-$ via WW
1Lbb [15]	Wino $\tilde{\chi}_1^\pm \tilde{\chi}_2^0$ via Wh
2LOJ [19]	Wino $\tilde{\chi}_1^+ \tilde{\chi}_1^-$ via WW, slepton pairs
2L2J [25]	Wino $\tilde{\chi}_1^\pm \tilde{\chi}_2^0$ via WZ
3L [23]	Wino $\tilde{\chi}_1^\pm \tilde{\chi}_2^0$ via WZ, Wino $\tilde{\chi}_1^\pm \tilde{\chi}_2^0$ via Wh , higgsino $\tilde{\chi}_1^\pm \tilde{\chi}_2^0 \tilde{\chi}_1^0$
4L [22]	Higgsino GGM
Compressed [20]	Wino $\tilde{\chi}_1^\pm \tilde{\chi}_2^0$ via WZ, higgsino $\tilde{\chi}_1^\pm \tilde{\chi}_2^0 \tilde{\chi}_1^0$
Disappearing-track [27]	Wino $\tilde{\chi}_1^+ \tilde{\chi}_1^-$ and $\tilde{\chi}_1^\pm \tilde{\chi}_1^0$

- **Reinterpretation using [ATLAS Full-Run2 EWK SUSY analyses!](#)**

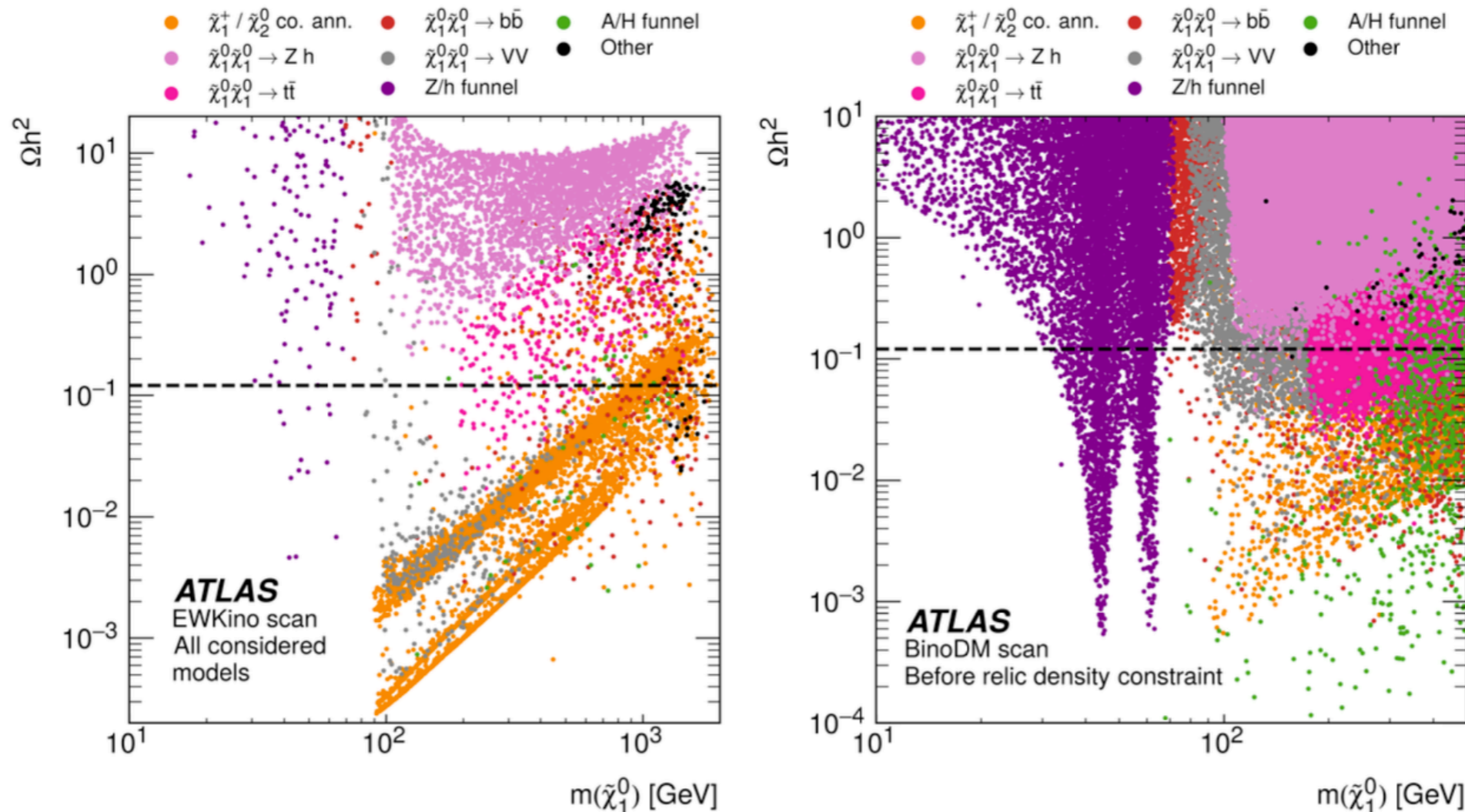
Scatter plot of models from “EWKino scan”



Bino-like LSP typically overestimate the DM relic density unless there are additional annihilation mechanisms available, not enough for study \rightarrow regenerate models specifically for “*BinoDM scan*”.

“EWKino scan” vs “BinoDM scan”

LSP- annihilation mechanism



(a) EWKino scan

(b) BinoDM scan

Higgsino/wino-like LSP, in general provides a DM relic density prediction below the measured value. They are by construction with enhanced co-annihilation with the chargino and/or neutralino2.

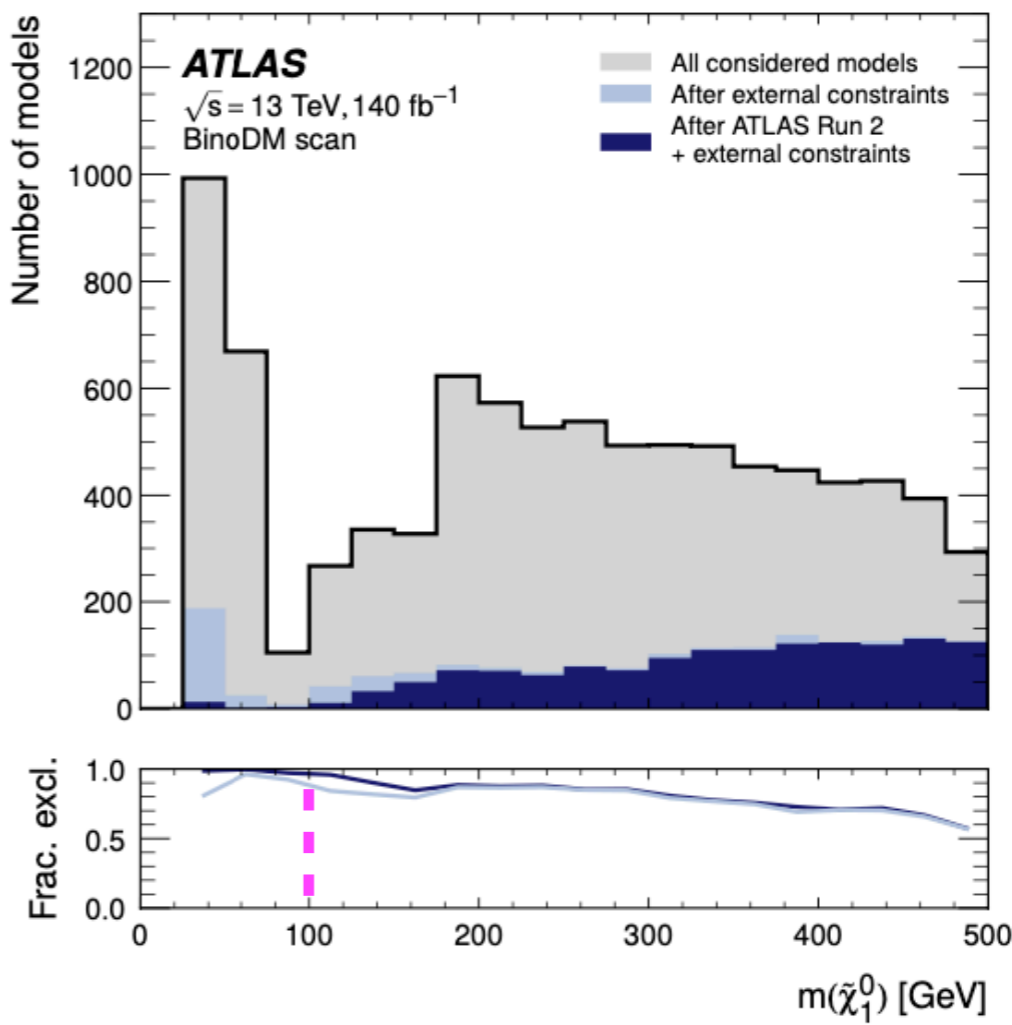
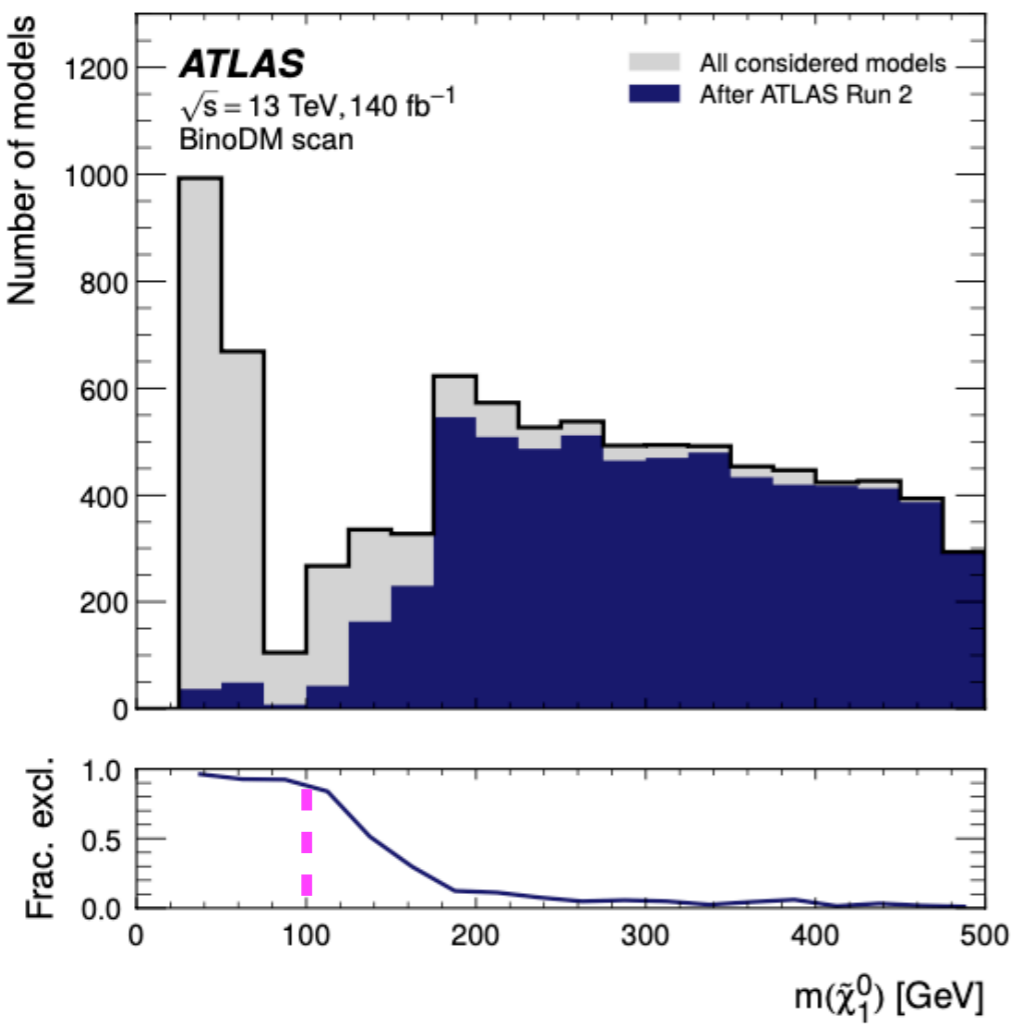
With significant statistics in BinoDM scan, after relic density constraint, dominant annihilation mechanism: Z/h funnel, C1/N2 co.ann, A/H funnel..

External Constraints

N.B. Additional external constraints complementary to the ATLAS search constraints are considered when discussing the results.

Category	Constraint	Lower bound	Upper bound	Notes
Flavour	$\mathcal{B}(b \rightarrow s\gamma)$	3.11×10^{-4}	3.87×10^{-4}	2022 PDG average (2σ window) [58]
	$\mathcal{B}(B_s \rightarrow \mu\mu)$	1.87×10^{-9}	4.31×10^{-9}	Most recent LHCb result (2σ window) [59]
	$\mathcal{B}(B^+ \rightarrow \tau\nu)$	6.10×10^{-5}	1.57×10^{-4}	2022 PDG average (2σ window) [58]
Precision electroweak	$\Delta\rho$	-0.0004	0.0018	Updated global electroweak fit by GFITTER group [60] (not including CDF W mass measurement [61])
	$\Gamma_{\text{inv}}^{\text{BSM}}(Z)$	-	2 MeV	Beyond-the-Standard Model contributions to precision electroweak measurements on the Z -resonance from experiments at the SLC and LEP colliders [62].
	$m(W)$	80.347 GeV	80.407 GeV	2022 PDG result (excluding CDF W mass measurement [61]) [58] but with the 2σ window expanded by 6 MeV to allow for uncertainty due to the top-quark mass in the MSSM Higgs calculation [63]
non-DM external constraints				
DM	Relic density	-	0.12	Latest bound from Planck [64]
	Direct detection $\sigma_{\text{Spin-independent}}$	DM constraints		Exclusion contour on direct detection of DM from the LZ Collaboration [65]
	Direct detection $\sigma_{\text{Spin-dependent}}$			Exclusion contour on direct detection of DM from PICO-60 [66]

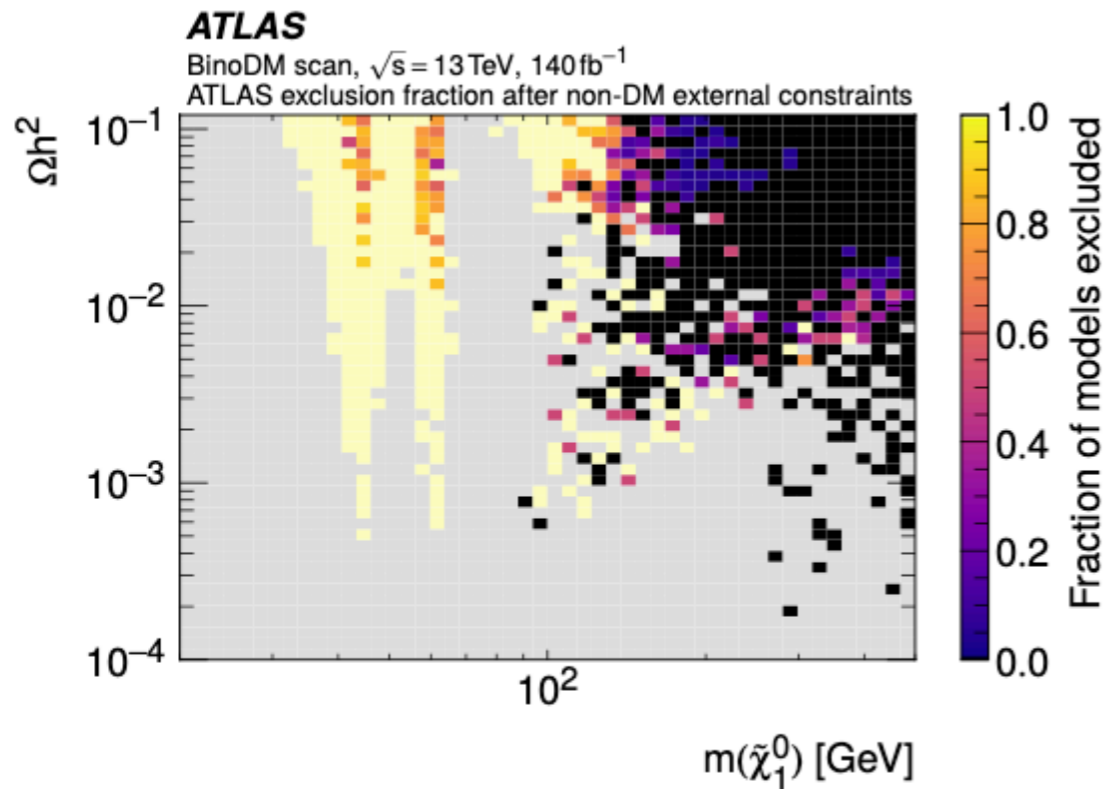
Constraints on the LSP mass



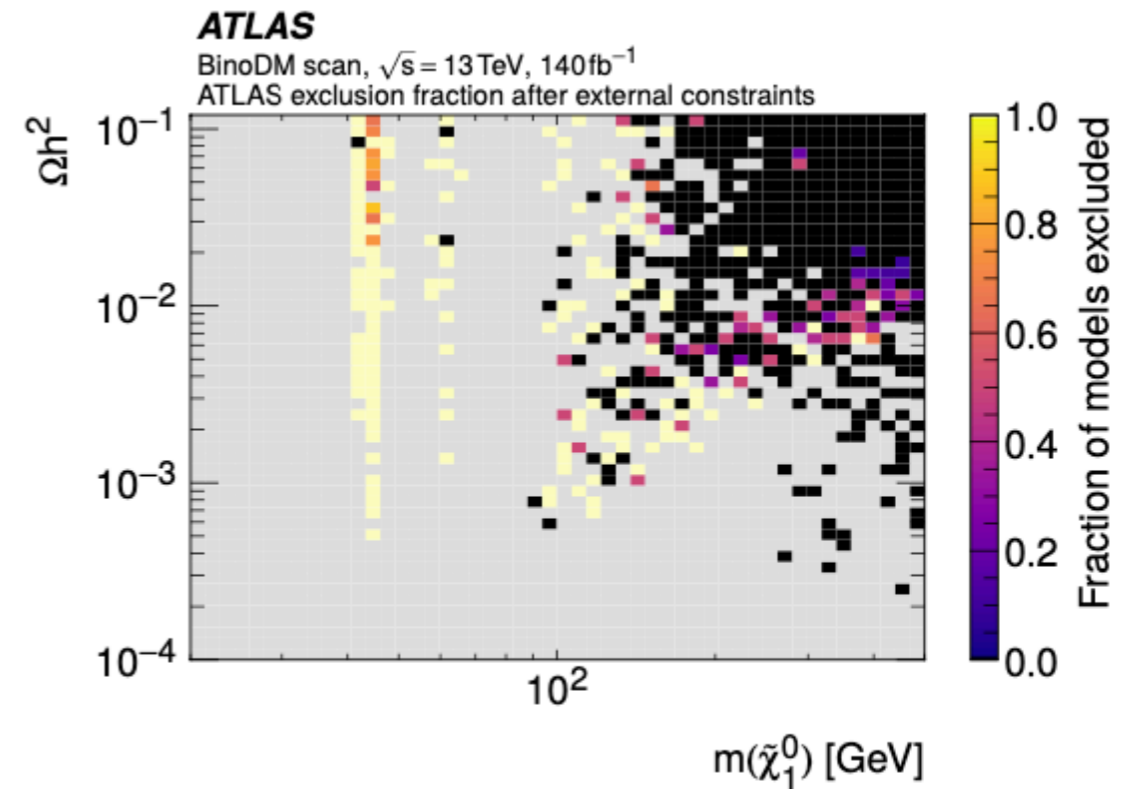
A bino-like LSP with a mass $< 100 \text{ GeV}$ is almost excluded by the ATLAS constraints, particularly when also considering external constraints.

Dark matter phenomenology

Color: *fraction of models excluded by the ATLAS Run 2 results*



(a) Models satisfying all non-DM constraints



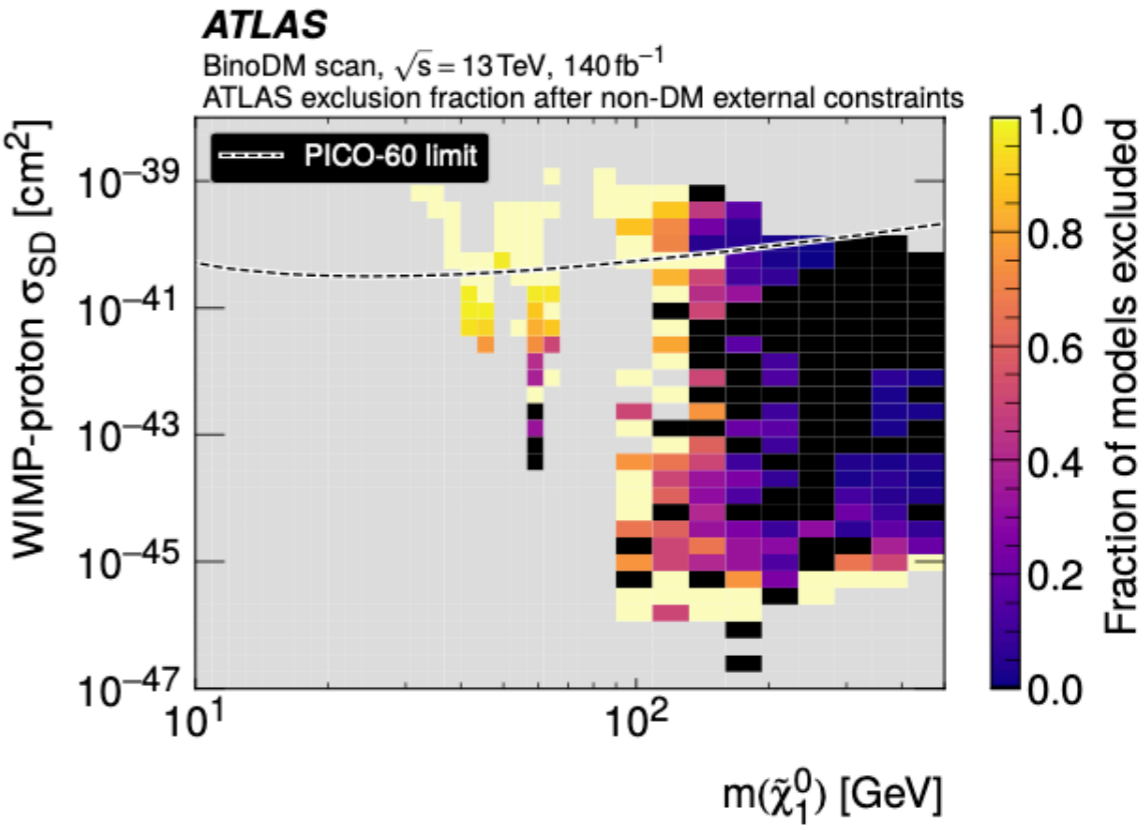
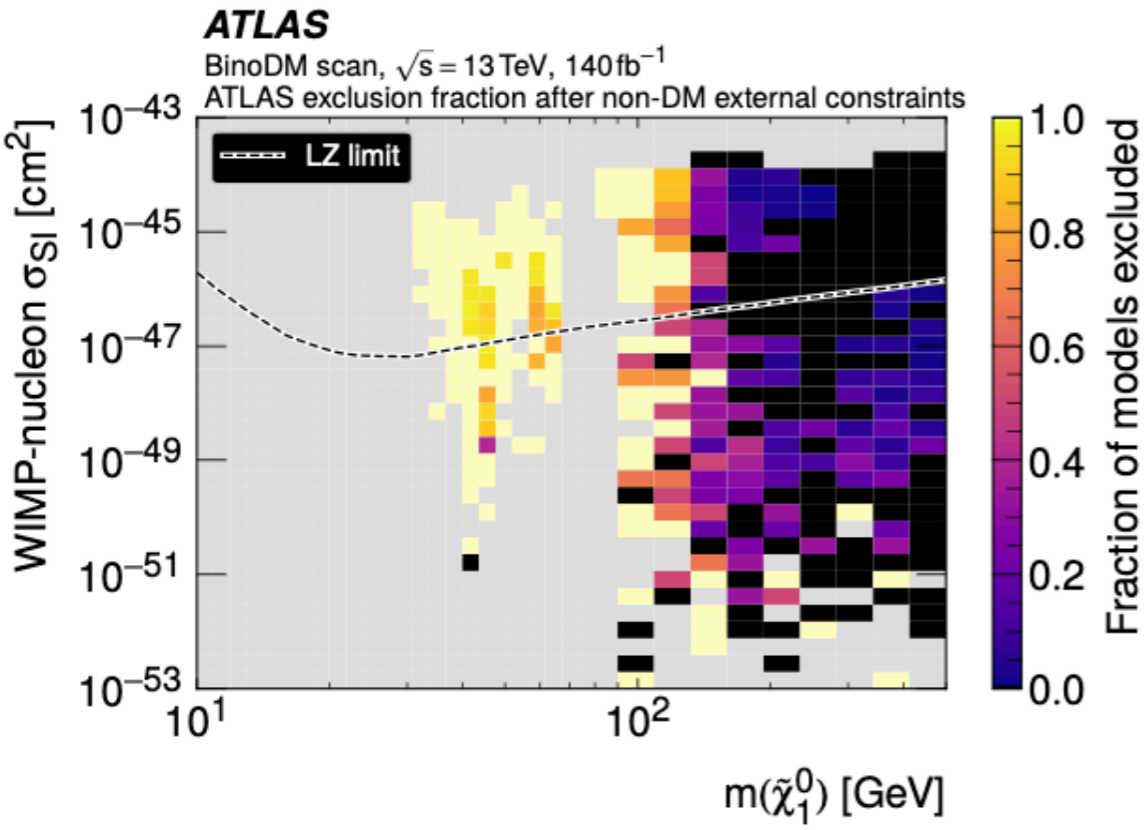
(b) Models satisfying all external constraints

The ATLAS constraints (from fraction color): stronger for funnel region; weaker at higher LSP masses

DM constraints (left fig \rightarrow right fig): strongly constrain the funnel regions, together with the ATLAS constraints only a few models remain viable there.

Collider VS Non-collider searches

Color: *fraction of models excluded by the ATLAS Run 2 results*

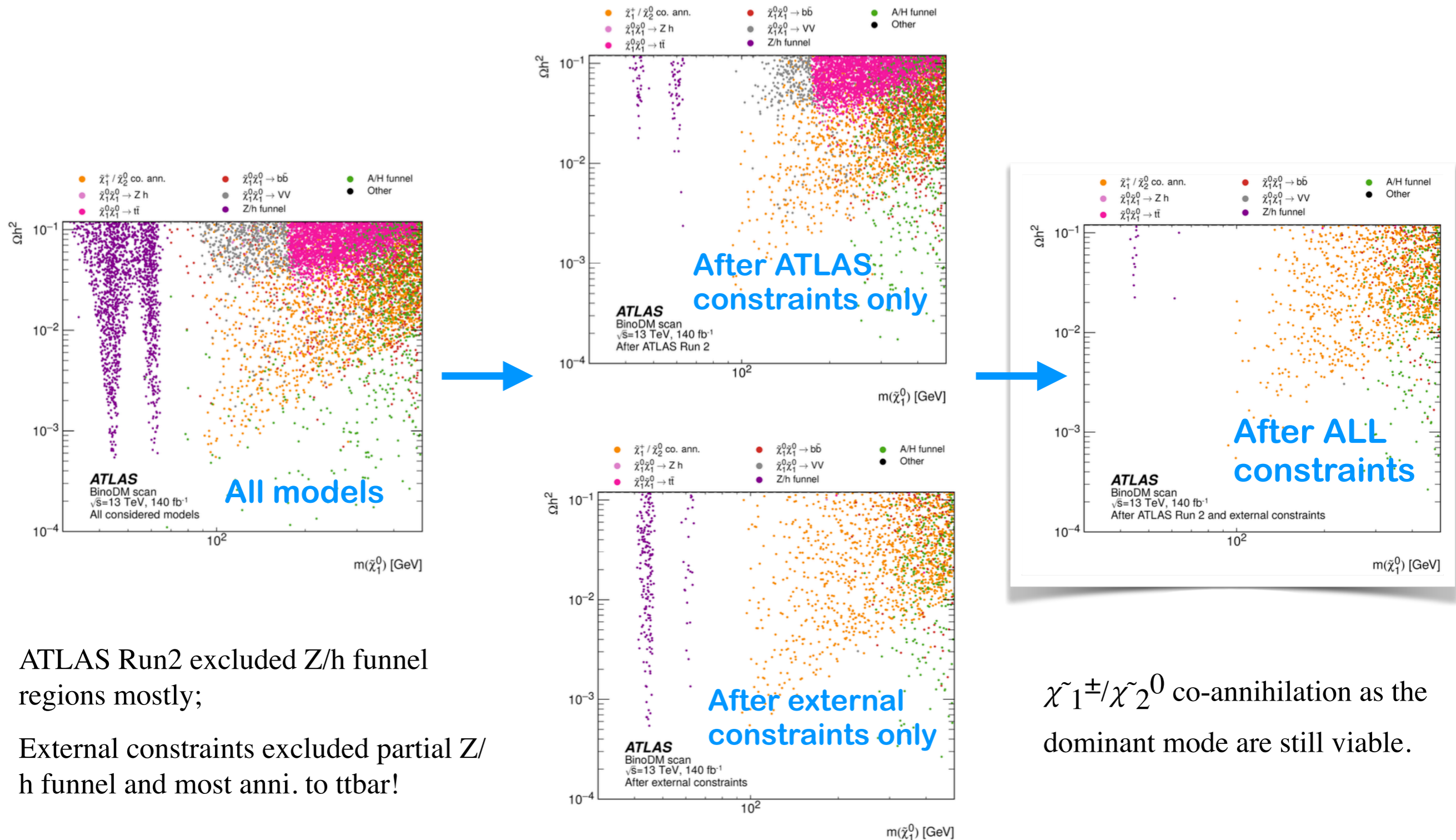


WIMP–nucleon/proton spin-independent /dependent scattering cross-sections vs LSP mass.

The LZ and PICO-60 upper limit contours shown in dashed lines as a comparison.

The ATLAS searches are observed to have a high sensitivity in regions where the direct-detection searches are insensitive and vice-versa, demonstrating the complementarity.

LSP- annihilation mechanism



ATLAS Run2 excluded Z/h funnel regions mostly;

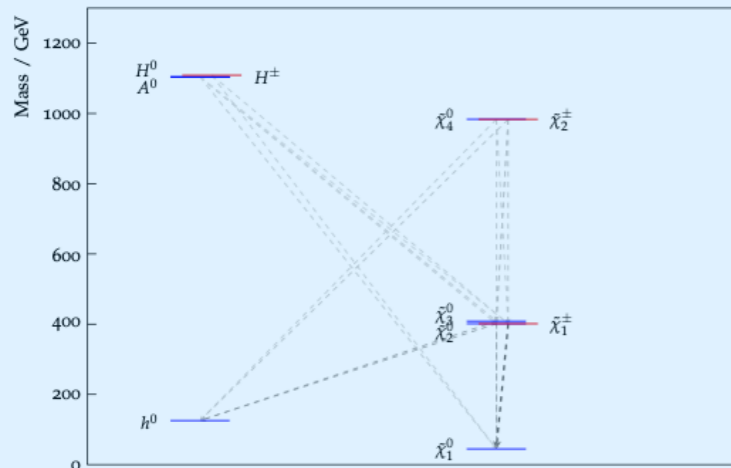
External constraints excluded partial Z/h funnel and most anni. to $t\bar{t}$!

$\tilde{\chi}_1^\pm / \tilde{\chi}_2^0$ co-annihilation as the dominant mode are still viable.

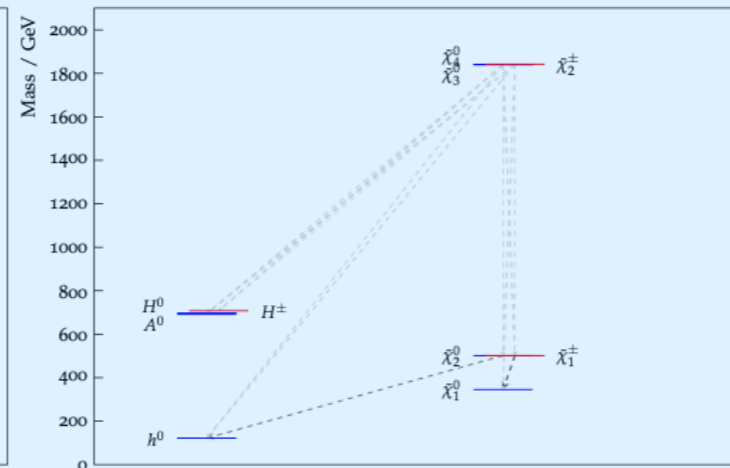
For fun :-)

Six benchmark models that survive ALL constraints.

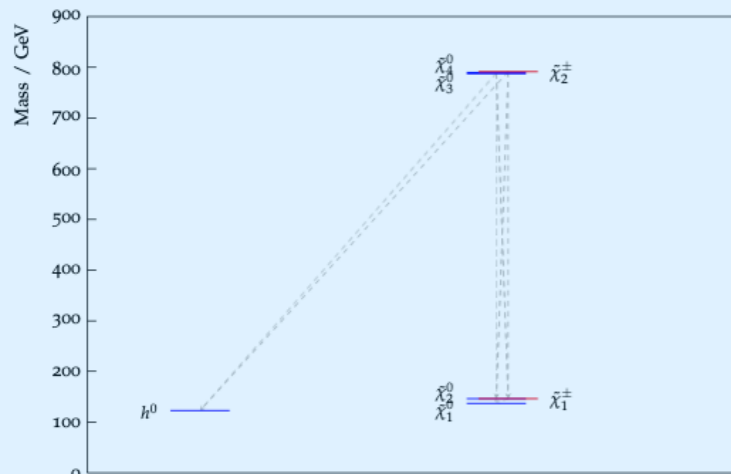
bino-like LSP



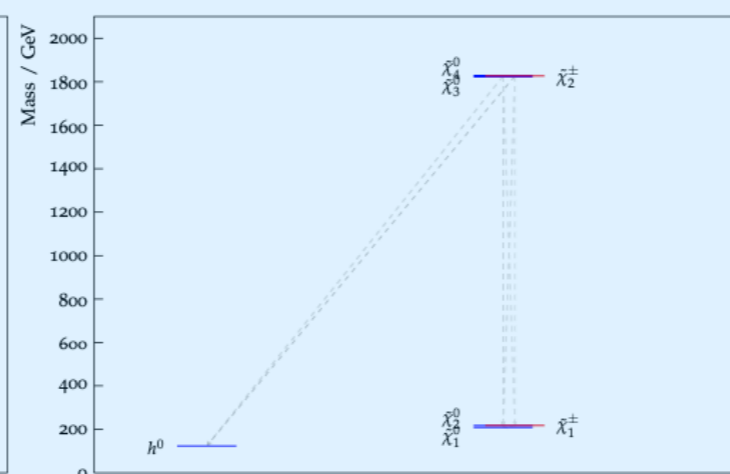
(a) Z/h funnel region



(b) A/H funnel region

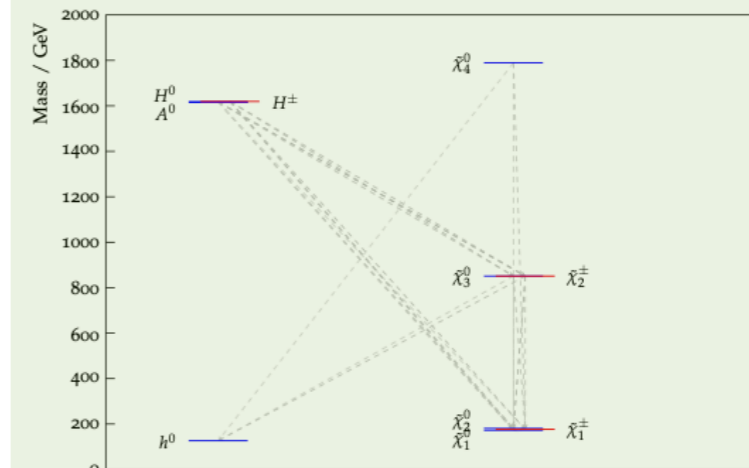


(c) Compressed region

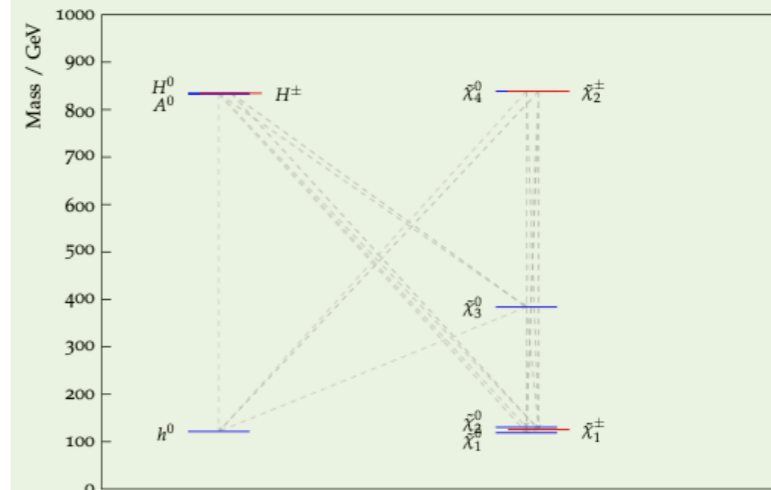


(d) Compressed region

Higgsino-like LSP



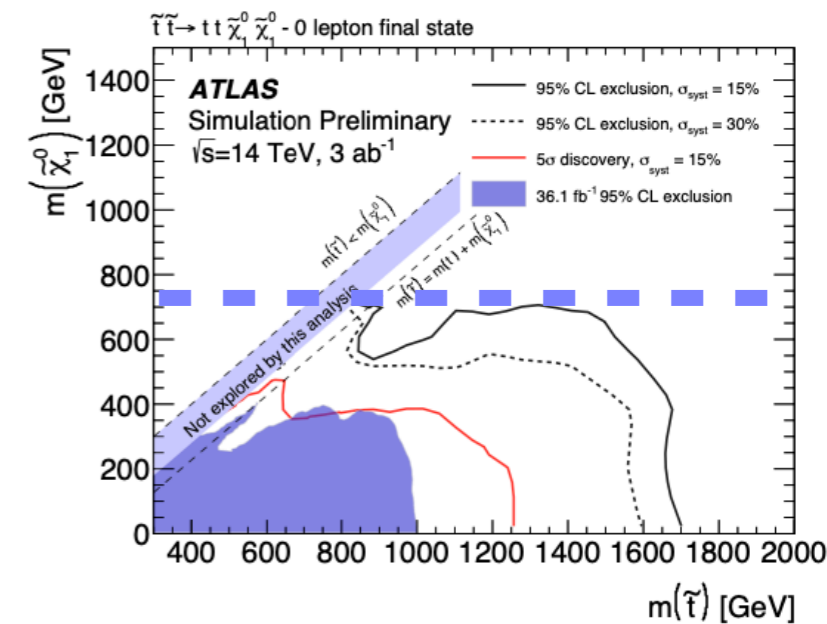
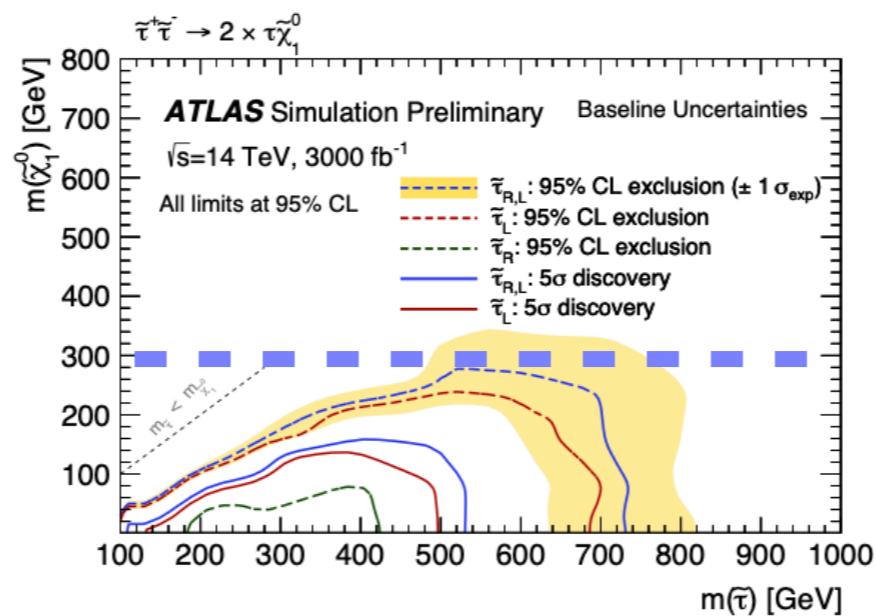
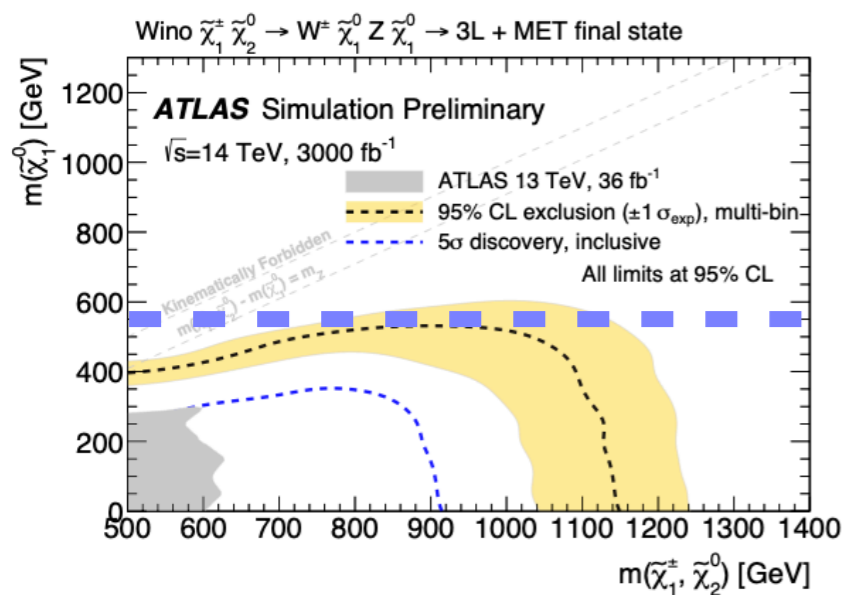
(a)



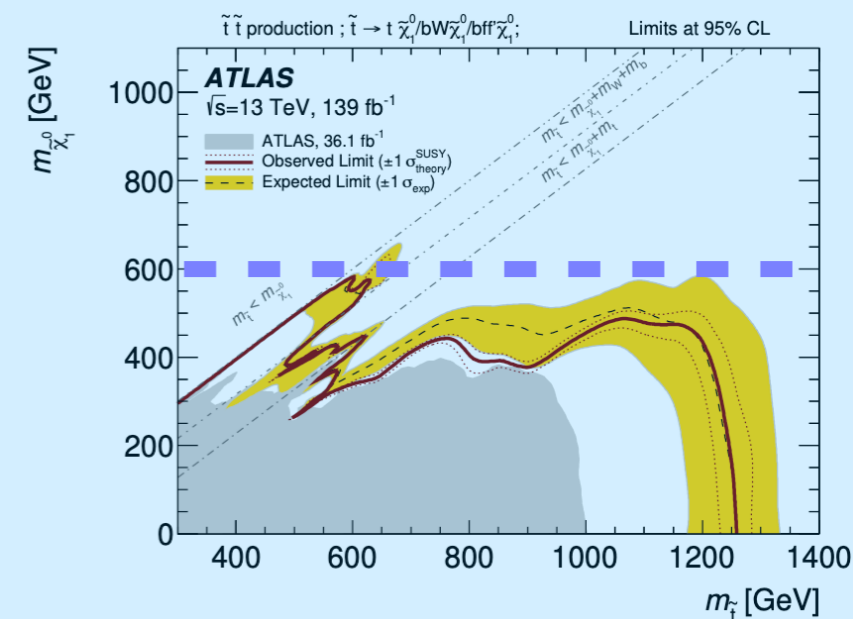
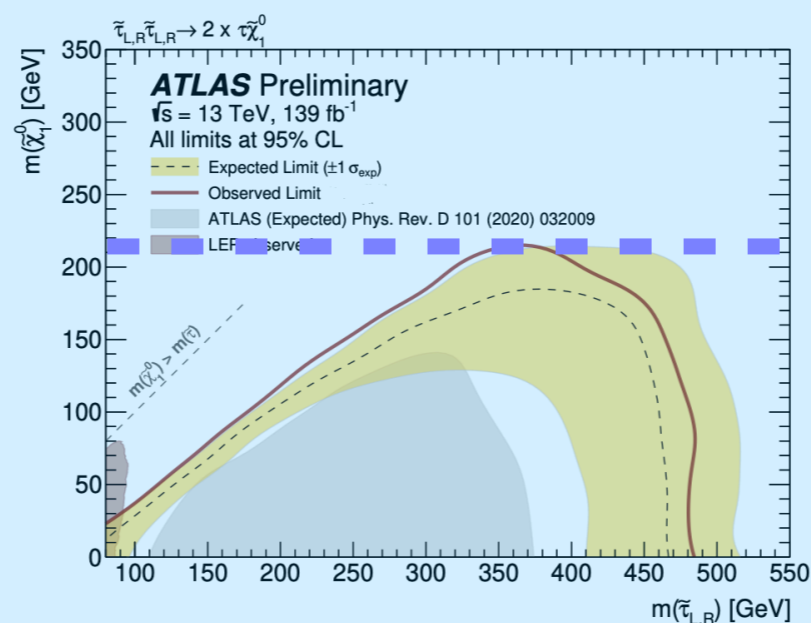
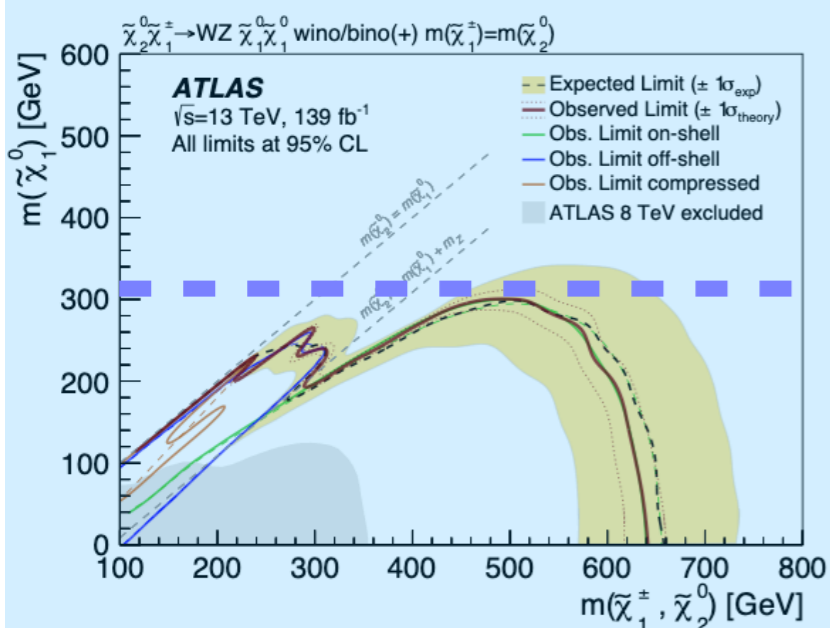
(b)

HL-LHC prospects

ATL-PHYS-PUB-2022-018

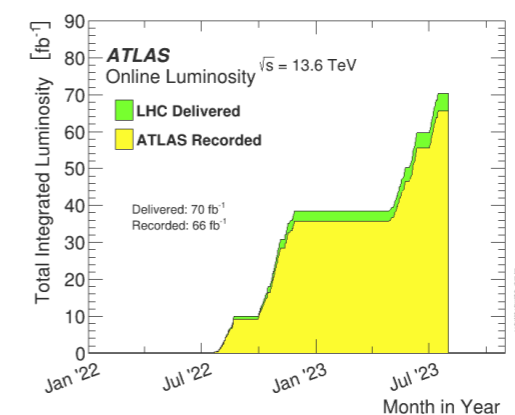


For 🍏-🍏 comparison, the corresponding similar analyses in Run2 are presented:



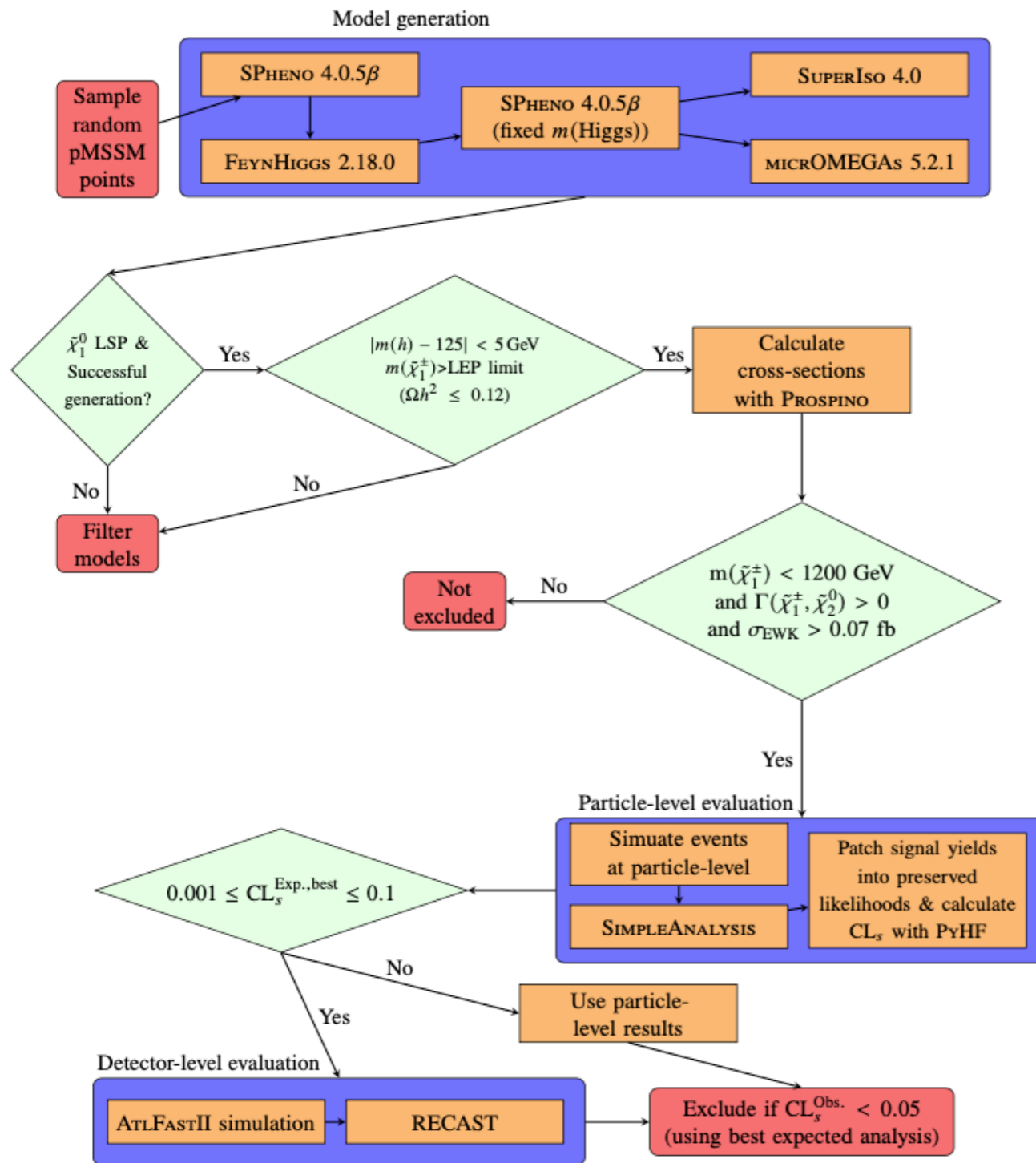
Summary

- **A quick overview of ATLAS full Run2 *RPC* SUSY search and a report on the latest EWK pMSSM results**
 - **The bounds on electroweakino masses are weaker in pMSSM comparing to the simplified models.**
 - **The impact of ATLAS searches on DM parameters (i.e. relic density, the scattering cross-sections) targeted by direct dark matter detection is presented.**
 - **Almost complete exclusion in the Z/h ‘funnel regions’ with all constraints.**
- **In (near) future,**
 - **Another pMSSM strong focusing on strongly produced SUSY searches is coming and expected to give us more hint**
 - **LHC Run3 data-taking is ongoing**
 - **More in HL-LHC**



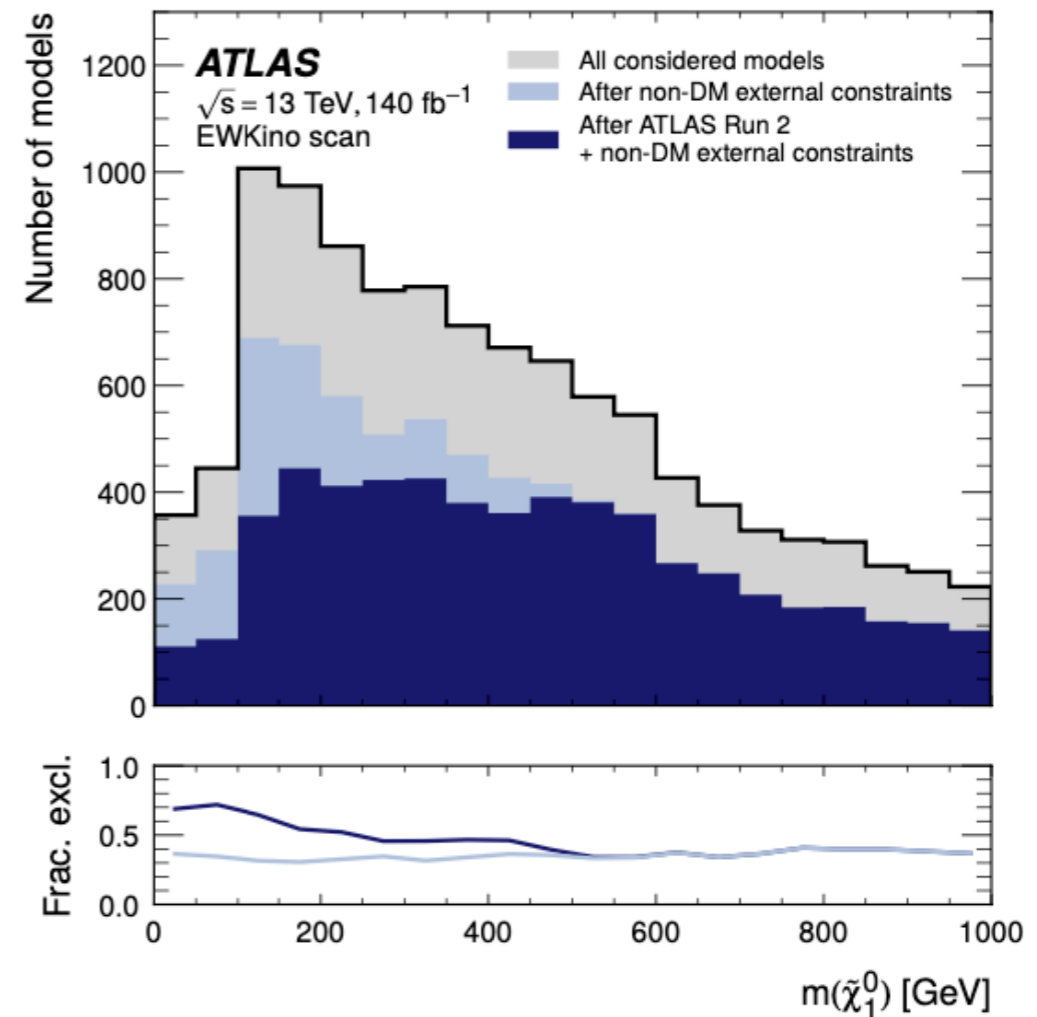
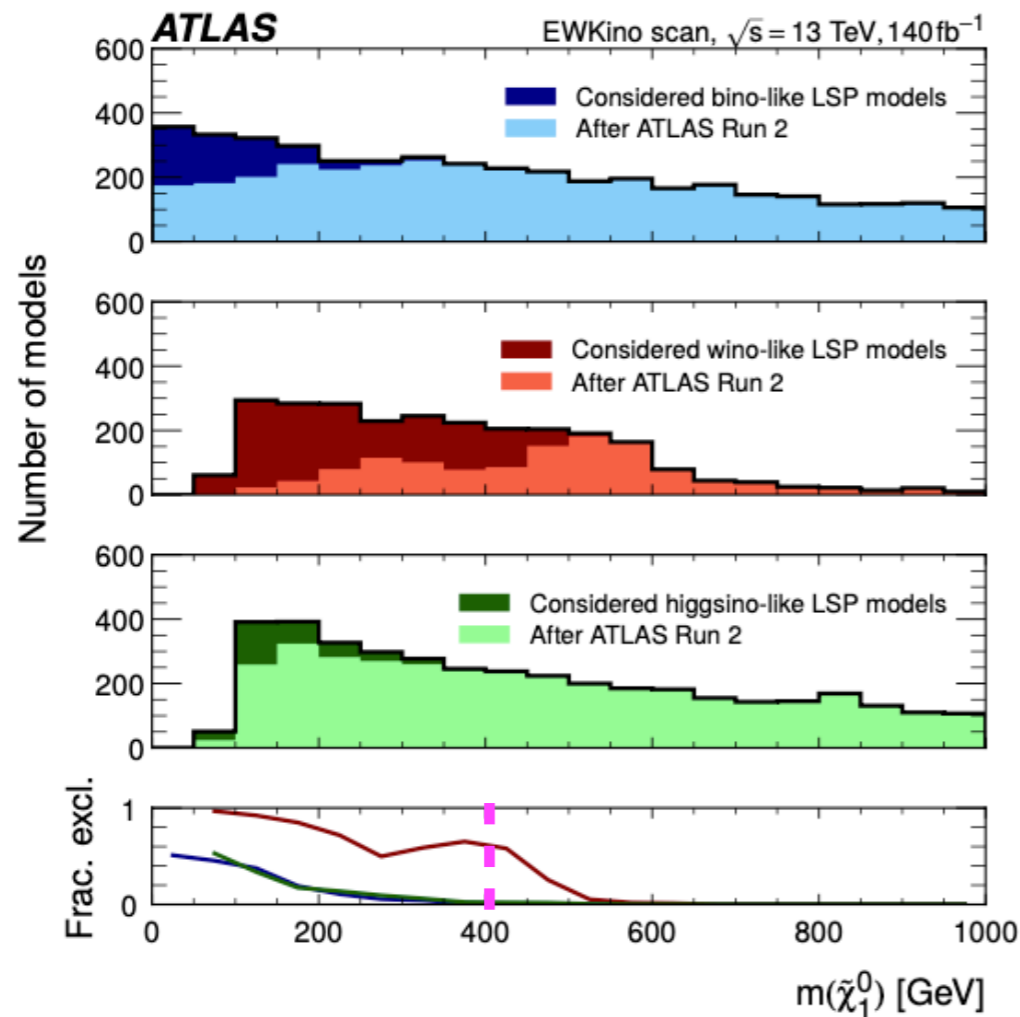
Extra slides

pMSSM technical workflow



- Using *CLs* as the discriminator
- Rely on particle-level evaluation as possible
- Otherwise move to detector-level evaluation using *RECAST*
- Eventually make a ‘*exclusion*’ decision for each model

Constraints on the LSP mass

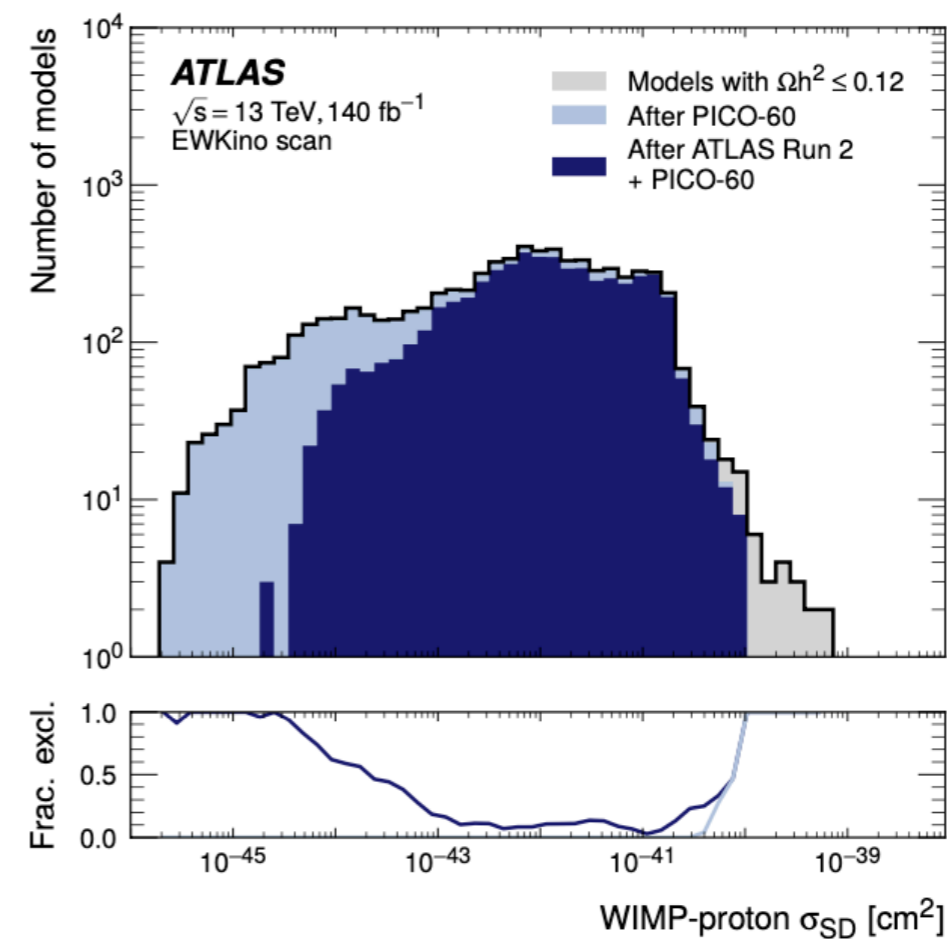
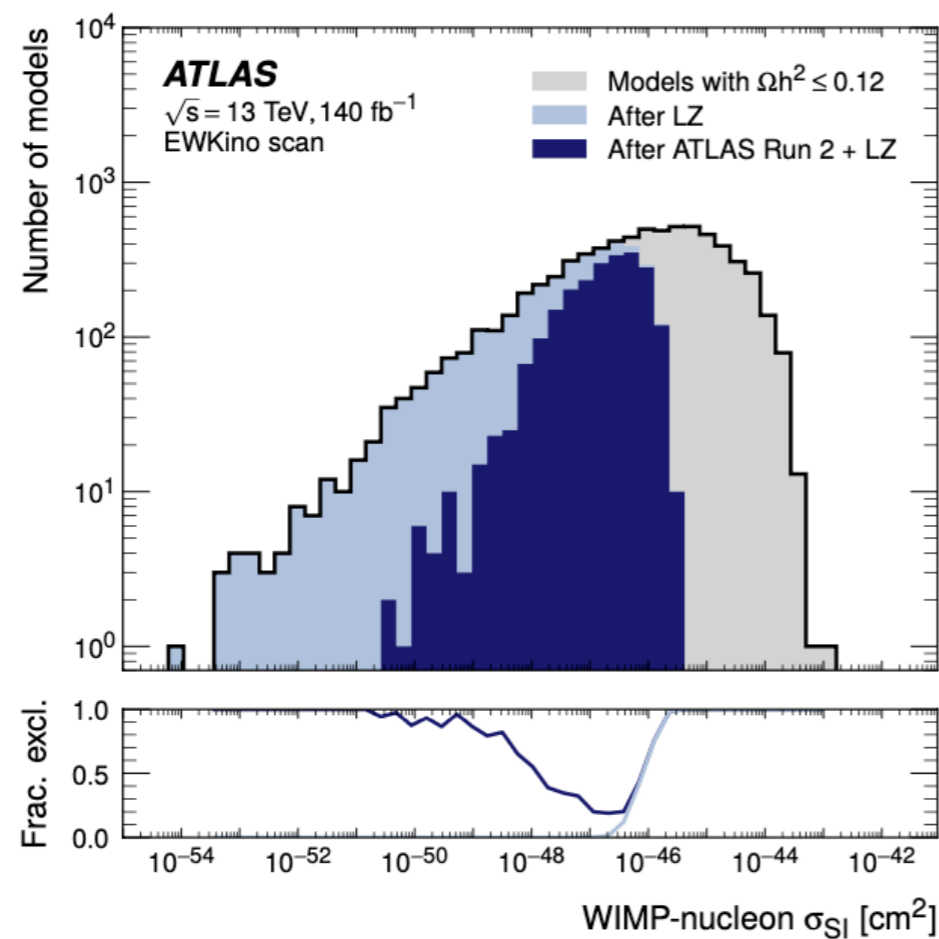


The impact of the ATLAS constraints is most significant at lower LSP mass!

The exclusion fractions are similar for bino-/higgsino-LSPs.

For an LSP < 400 GeV, the ATLAS Run 2 searches exclude more than 50% of the wino LSP models.

Complementarity between DM and ATLAS Run 2 constraints



ATLAS provides good exclusion of low cross-section scenarios that lie well below the LZ and PICO-60 limits.

ATLAS SUSY Searches* - 95% CL Lower Limits

August 2023

ATLAS Preliminary

$\sqrt{s} = 13$ TeV

Model	Signature	$\int \mathcal{L} dt [\text{fb}^{-1}]$	Mass limit	Reference		
Inclusive Searches	$\tilde{q}\tilde{q}, \tilde{q} \rightarrow q\tilde{\chi}_1^0$	0 e, μ	2-6 jets E_T^{miss} 140	\tilde{q} [1x, 8x Degen.] 1.0 1.85	$m(\tilde{\chi}_1^0) < 400$ GeV	
		mono-jet	1-3 jets E_T^{miss} 140	\tilde{q} [8x Degen.] 0.9	$m(\tilde{q}) - m(\tilde{\chi}_1^0) = 5$ GeV	
	$\tilde{g}\tilde{g}, \tilde{g} \rightarrow q\tilde{q}\tilde{\chi}_1^0$	0 e, μ	2-6 jets E_T^{miss} 140	\tilde{g} 2.3	$m(\tilde{\chi}_1^0) = 0$ GeV	
				Forbidden 1.15-1.95	$m(\tilde{\chi}_1^0) = 1000$ GeV	
	$\tilde{g}\tilde{g}, \tilde{g} \rightarrow q\tilde{q}W\tilde{\chi}_1^0$	1 e, μ	2-6 jets	E_T^{miss} 140	\tilde{g} 2.2	$m(\tilde{\chi}_1^0) < 600$ GeV
	$\tilde{g}\tilde{g}, \tilde{g} \rightarrow q\tilde{q}(\ell\ell)\tilde{\chi}_1^0$	$ee, \mu\mu$	2 jets E_T^{miss} 140	\tilde{g} 2.2	$m(\tilde{\chi}_1^0) < 700$ GeV	
3 rd gen. squarks direct production	$\tilde{t}_1\tilde{t}_1, \tilde{t}_1 \rightarrow t\tilde{\chi}_1^0$	0 e, μ	≥ 1 jet E_T^{miss} 140	\tilde{t}_1 1.25	$m(\tilde{\chi}_1^0) = 1$ GeV	
	$\tilde{t}_1\tilde{t}_1, \tilde{t}_1 \rightarrow Wb\tilde{\chi}_1^0$	1 e, μ	3 jets/1 b E_T^{miss} 140	\tilde{t}_1 1.05	$m(\tilde{\chi}_1^0) = 500$ GeV	
	$\tilde{t}_1\tilde{t}_1, \tilde{t}_1 \rightarrow \tilde{\tau}_1 b\nu, \tilde{\tau}_1 \rightarrow \tau\tilde{G}$	1-2 τ	2 jets/1 b E_T^{miss} 140	\tilde{t}_1 1.4	$m(\tilde{\tau}_1) = 800$ GeV	
	$\tilde{t}_1\tilde{t}_1, \tilde{t}_1 \rightarrow c\tilde{\chi}_1^0 / \tilde{c}\tilde{c}, \tilde{c} \rightarrow c\tilde{\chi}_1^0$	0 e, μ	2 c E_T^{miss} 36.1	\tilde{t}_1 0.85	$m(\tilde{\chi}_1^0) = 0$ GeV	
	$\tilde{t}_1\tilde{t}_1, \tilde{t}_1 \rightarrow c\tilde{\chi}_1^0 / \tilde{c}\tilde{c}, \tilde{c} \rightarrow c\tilde{\chi}_1^0$	0 e, μ	mono-jet E_T^{miss} 140	\tilde{t}_1 0.55	$m(\tilde{t}_1, \tilde{c}) - m(\tilde{\chi}_1^0) = 5$ GeV	
	$\tilde{t}_1\tilde{t}_1, \tilde{t}_1 \rightarrow t\tilde{\chi}_2^0, \tilde{\chi}_2^0 \rightarrow Z/h\tilde{\chi}_1^0$	1-2 e, μ	1-4 b E_T^{miss} 140	\tilde{t}_1 0.067-1.18	$m(\tilde{\chi}_1^0) = 500$ GeV	
	$\tilde{t}_2\tilde{t}_2, \tilde{t}_2 \rightarrow \tilde{t}_1 + Z$	3 e, μ	1 b E_T^{miss} 140	\tilde{t}_2 0.86	$m(\tilde{\chi}_1^0) = 360$ GeV, $m(\tilde{t}_1) - m(\tilde{\chi}_1^0) = 40$ GeV	
EW direct	$\tilde{\chi}_1^+\tilde{\chi}_2^0$ via WZ	Multiple ℓ /jets	≥ 1 jet E_T^{miss} 140	$\tilde{\chi}_1^+/\tilde{\chi}_2^0$ 0.96	$m(\tilde{\chi}_1^0) = 0$, wino-bino	
		$ee, \mu\mu$		$\tilde{\chi}_1^+/\tilde{\chi}_2^0$ 0.205	$m(\tilde{\chi}_1^+) - m(\tilde{\chi}_1^0) = 5$ GeV, wino-bino	
	$\tilde{\chi}_1^+\tilde{\chi}_1^0$ via WW	2 e, μ	E_T^{miss} 140	$\tilde{\chi}_1^+$ 0.42	$m(\tilde{\chi}_1^0) = 0$, wino-bino	
	$\tilde{\chi}_1^+\tilde{\chi}_2^0$ via Wh	Multiple ℓ /jets	E_T^{miss} 140	$\tilde{\chi}_1^+/\tilde{\chi}_2^0$ 1.06	$m(\tilde{\chi}_1^0) = 70$ GeV, wino-bino	
	$\tilde{\chi}_1^+\tilde{\chi}_1^0$ via $\tilde{\ell}_L/\tilde{\nu}$	2 e, μ	E_T^{miss} 140	$\tilde{\chi}_1^+$ 1.0	$m(\tilde{\ell}, \tilde{\nu}) = 0.5(m(\tilde{\chi}_1^+) + m(\tilde{\chi}_1^0))$	
	$\tilde{\tau}\tilde{\tau}, \tilde{\tau} \rightarrow \tau\tilde{\chi}_1^0$	2 τ	E_T^{miss} 140	$\tilde{\tau}$ [R, L] 0.34 0.48	$m(\tilde{\chi}_1^0) = 0$	
	$\tilde{\ell}_{L,R}\tilde{\ell}_{L,R}, \tilde{\ell} \rightarrow \ell\tilde{\chi}_1^0$	2 e, μ	0 jets E_T^{miss} 140	$\tilde{\ell}$ 0.7	$m(\tilde{\chi}_1^0) = 0$	
		$ee, \mu\mu$	≥ 1 jet E_T^{miss} 140	$\tilde{\ell}$ 0.26	$m(\tilde{\ell}) - m(\tilde{\chi}_1^0) = 10$ GeV	
$\tilde{H}\tilde{H}, \tilde{H} \rightarrow h\tilde{G}/Z\tilde{G}$	0 e, μ	≥ 3 b E_T^{miss} 140	\tilde{H} 0.94	$\text{BR}(\tilde{\chi}_1^0 \rightarrow h\tilde{G}) = 1$		
	4 e, μ	0 jets E_T^{miss} 140	\tilde{H} 0.55	$\text{BR}(\tilde{\chi}_1^0 \rightarrow Z\tilde{G}) = 1$		
	0 e, μ	≥ 2 large jets E_T^{miss} 140	\tilde{H} 0.45-0.93	$\text{BR}(\tilde{\chi}_1^0 \rightarrow Z\tilde{G}) = 1$		
	2 e, μ	≥ 2 jets E_T^{miss} 140	\tilde{H} 0.77	$\text{BR}(\tilde{\chi}_1^0 \rightarrow Z\tilde{G}) = \text{BR}(\tilde{\chi}_1^0 \rightarrow h\tilde{G}) = 0.5$		
Long-lived particles	Direct $\tilde{\chi}_1^+\tilde{\chi}_1^-$ prod., long-lived $\tilde{\chi}_1^\pm$	Disapp. trk	1 jet E_T^{miss} 140	$\tilde{\chi}_1^\pm$ 0.66	Pure Wino	
				$\tilde{\chi}_1^\pm$ 0.21	Pure higgsino	
	Stable \tilde{g} R-hadron	pixel dE/dx	E_T^{miss} 140	\tilde{g} 2.05		
	Metastable \tilde{g} R-hadron, $\tilde{g} \rightarrow q\tilde{q}\tilde{\chi}_1^0$	pixel dE/dx	E_T^{miss} 140	\tilde{g} [$\tau(\tilde{g}) = 10$ ns]	$m(\tilde{\chi}_1^0) = 100$ GeV	
	$\tilde{\ell}\tilde{\ell}, \tilde{\ell} \rightarrow \ell\tilde{G}$	Displ. lep	E_T^{miss} 140	$\tilde{\ell}, \tilde{\mu}$ 0.7	$\tau(\tilde{\ell}) = 0.1$ ns	
	pixel dE/dx	E_T^{miss} 140	$\tilde{\tau}$ 0.34 0.36	$\tau(\tilde{\ell}) = 0.1$ ns		
			$\tilde{\tau}$ 0.36	$\tau(\tilde{\ell}) = 10$ ns		
RPV	$\tilde{\chi}_1^+\tilde{\chi}_1^0/\tilde{\chi}_1^+\tilde{\chi}_1^0, \tilde{\chi}_1^+ \rightarrow Z\ell\ell\ell$	3 e, μ	E_T^{miss} 140	$\tilde{\chi}_1^+/\tilde{\chi}_1^0$ [BR(Z τ)=1, BR(Z e)=1] 0.625 1.05	Pure Wino	
	$\tilde{\chi}_1^+\tilde{\chi}_1^0/\tilde{\chi}_2^0 \rightarrow WW/Z\ell\ell\ell\nu\nu$	4 e, μ	E_T^{miss} 140	$\tilde{\chi}_1^+/\tilde{\chi}_2^0$ [$\lambda_{33} \neq 0, \lambda_{23} \neq 0$] 0.95 1.55	$m(\tilde{\chi}_1^0) = 200$ GeV	
	$\tilde{g}\tilde{g}, \tilde{g} \rightarrow q\tilde{q}\tilde{\chi}_1^0, \tilde{\chi}_1^0 \rightarrow q\tilde{q}\tilde{\chi}_1^0$	≥ 8 jets	E_T^{miss} 140	\tilde{g} [$m(\tilde{\chi}_1^0) = 50$ GeV, 1250 GeV] 1.6 2.25	Large λ'_{112}	
	$\tilde{u}, \tilde{t} \rightarrow t\tilde{\chi}_1^0, \tilde{\chi}_1^0 \rightarrow t\tilde{b}s$	Multiple	36.1	\tilde{t} [$\lambda'_{333} = 2e-4, 1e-2$] 0.55 1.05	$m(\tilde{\chi}_1^0) = 200$ GeV, bino-like	
	$\tilde{u}, \tilde{t} \rightarrow b\tilde{\chi}_1^+, \tilde{\chi}_1^+ \rightarrow b\tilde{b}s$	$\geq 4b$	140	\tilde{t} Forbidden 0.95	$m(\tilde{\chi}_1^+) = 500$ GeV	
	$\tilde{t}_1\tilde{t}_1, \tilde{t}_1 \rightarrow b\tilde{s}$	2 jets + 2 b	36.7	\tilde{t}_1 [$q\tilde{q}, b\tilde{s}$] 0.42 0.61		
	$\tilde{t}_1\tilde{t}_1, \tilde{t}_1 \rightarrow q\tilde{\ell}$	2 e, μ	2 b 36.1	\tilde{t}_1 0.4-1.45	$\text{BR}(\tilde{t}_1 \rightarrow b\tilde{e}/b\tilde{\mu}) > 20\%$	
	1 μ	DV 136	\tilde{t}_1 [1e-10 < $\lambda'_{234} < 1e-8, 3e-10 < \lambda'_{234} < 3e-9$] 1.0 1.6	$\text{BR}(\tilde{t}_1 \rightarrow q\tilde{\mu}) = 100\%, \cos\theta_1 = 1$		
$\tilde{\chi}_1^+/\tilde{\chi}_2^0/\tilde{\chi}_1^0, \tilde{\chi}_{1,2}^0 \rightarrow t\tilde{b}s, \tilde{\chi}_1^+ \rightarrow b\tilde{b}s$	1-2 e, μ	≥ 6 jets	E_T^{miss} 140	$\tilde{\chi}_1^0$ 0.2-0.32	Pure higgsino	

10^{-1}

1

Mass scale [TeV]

*Only a selection of the available mass limits on new states or phenomena is shown. Many of the limits are based on simplified models, c.f. refs. for the assumptions made.

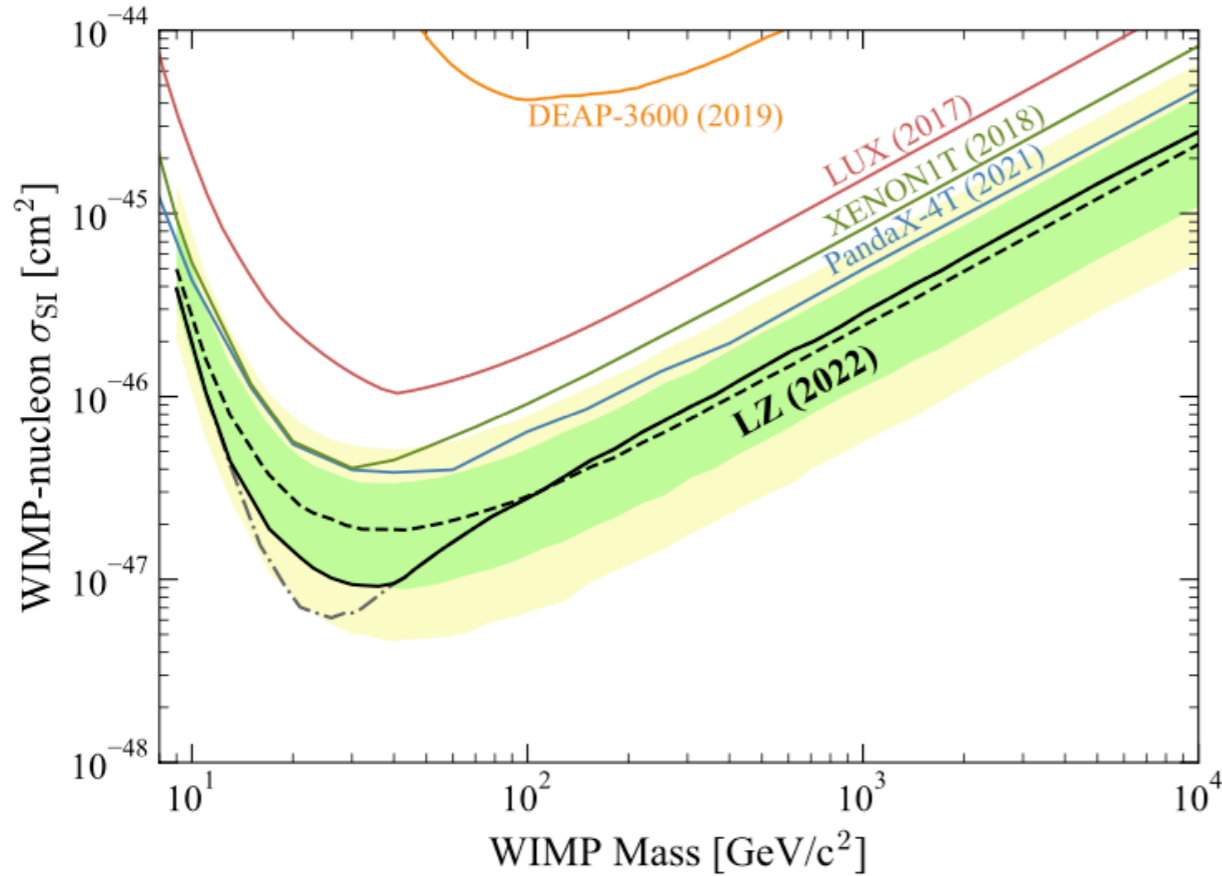


FIG. 5. The 90% confidence limit (black line) for the spin-independent WIMP cross section vs. WIMP mass. The gray dot-dash line shows the limit before applying the power constraint described in the text. The green and yellow bands are the 1σ and 2σ sensitivity bands. The dotted line shows the median of the sensitivity projection. Also shown are the PandaX-4T [26], XENON1T [25], LUX [28], and DEAP-3600 [75] limits.

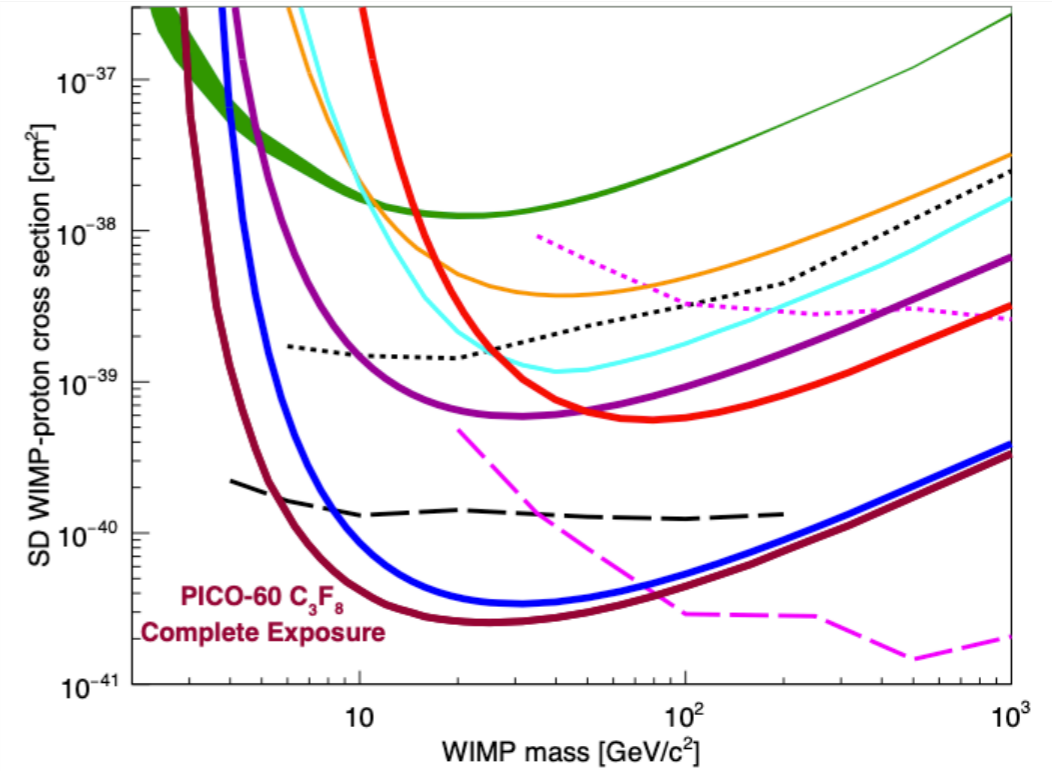
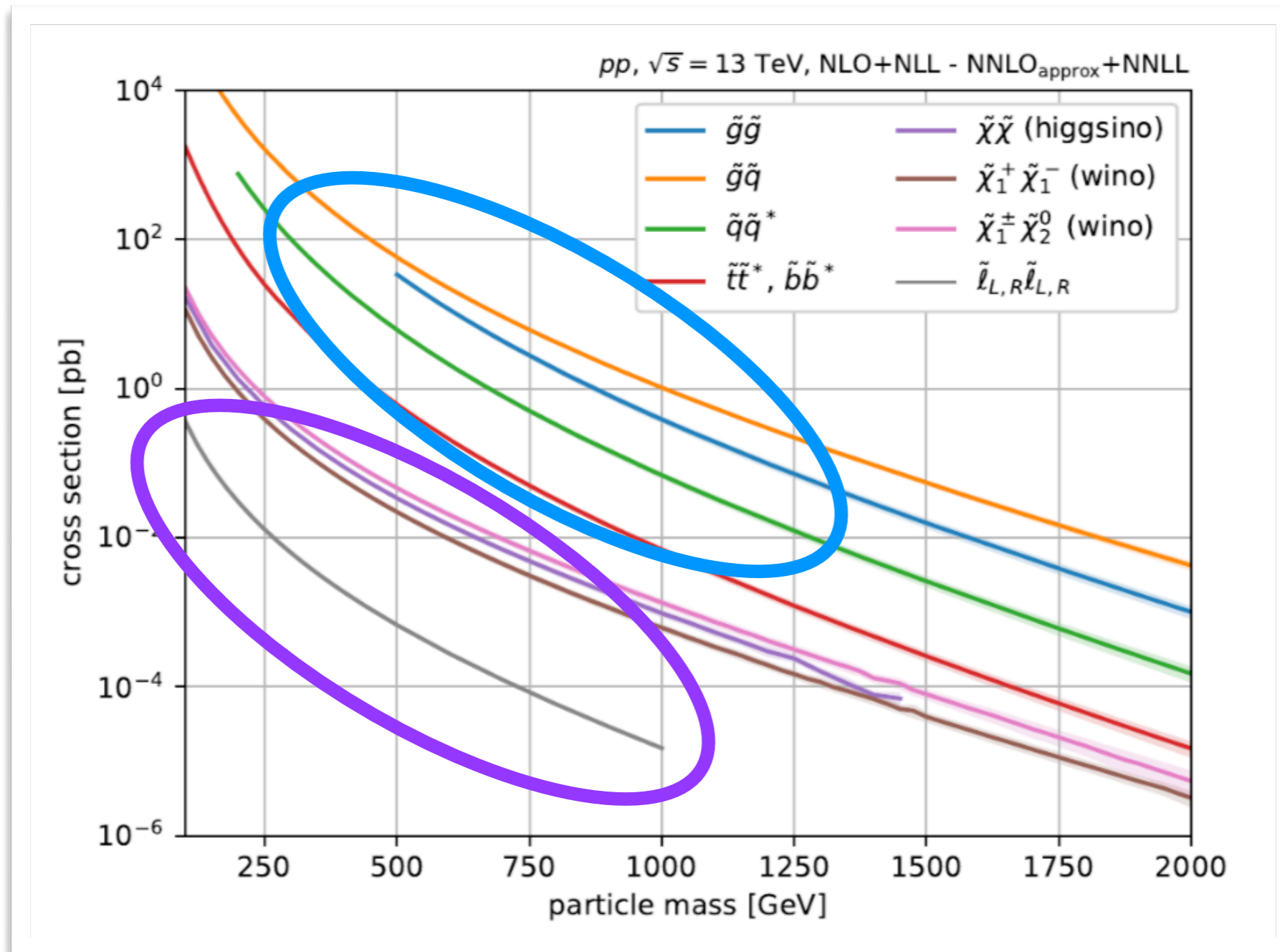


FIG. 7. The 90% C.L. limit on the SD WIMP-proton cross section from the profile likelihood analysis of the PICO-60 C_3F_8 combined blind exposure plotted in thick maroon, along with limits from the first blind exposure of PICO-60 C_3F_8 (thick blue) [14], as well as limits from PICO-60 CF_3I (thick red) [11], PICO-2L (thick purple) [10], PICASSO (green band) [20], SIMPLE (orange) [21], PandaX-II (cyan) [46], IceCube (dashed and dotted pink) [47], and SuperK (dashed and dotted black) [48, 49]. The indirect limits from IceCube and SuperK assume annihilation to τ leptons (dashed) and b quarks (dotted). Additional limits, not shown for clarity, are set by LUX [51] and XENON1T [53] (comparable to PandaX-II) and by ANTARES [54, 55] (comparable to IceCube).

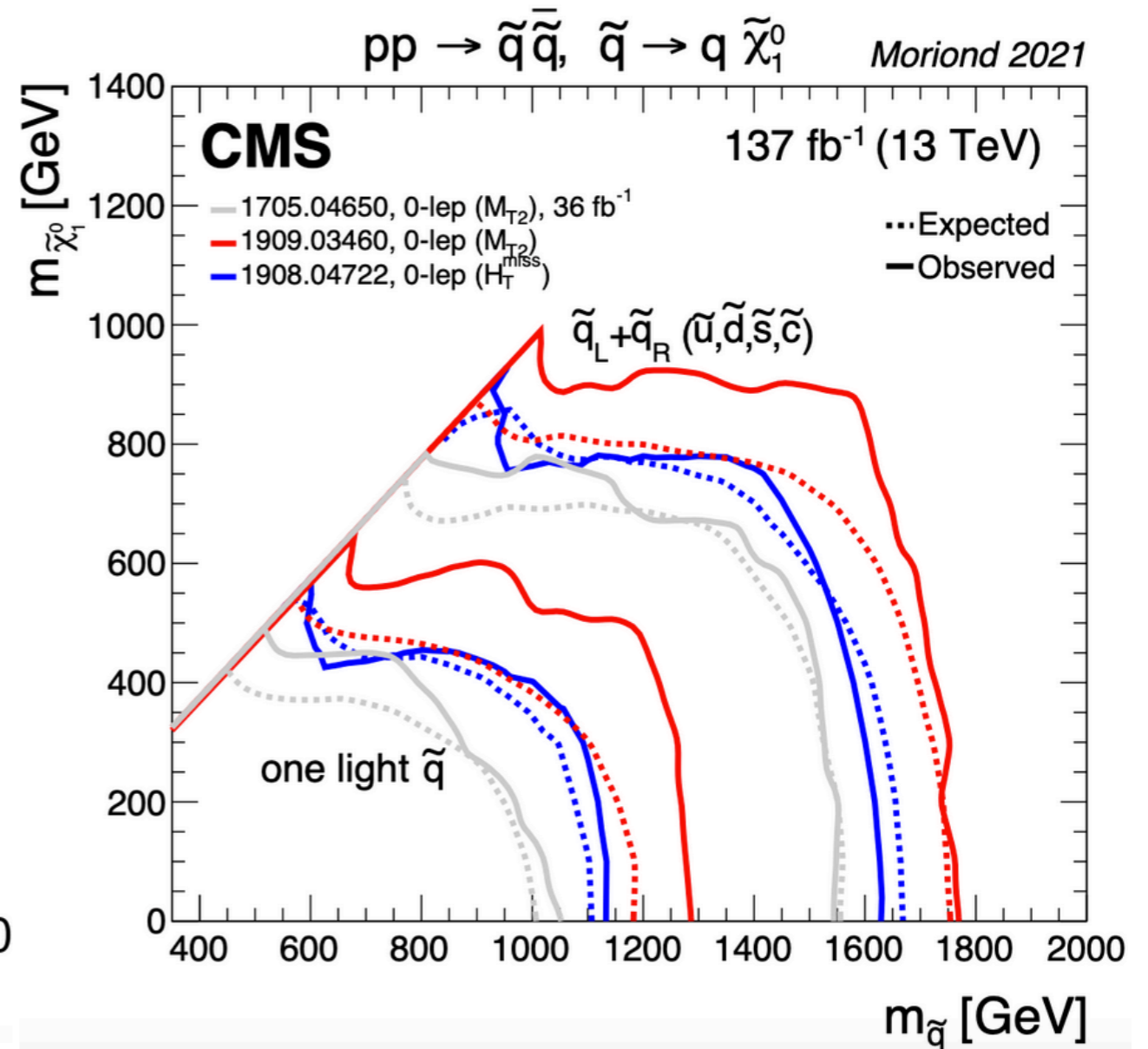
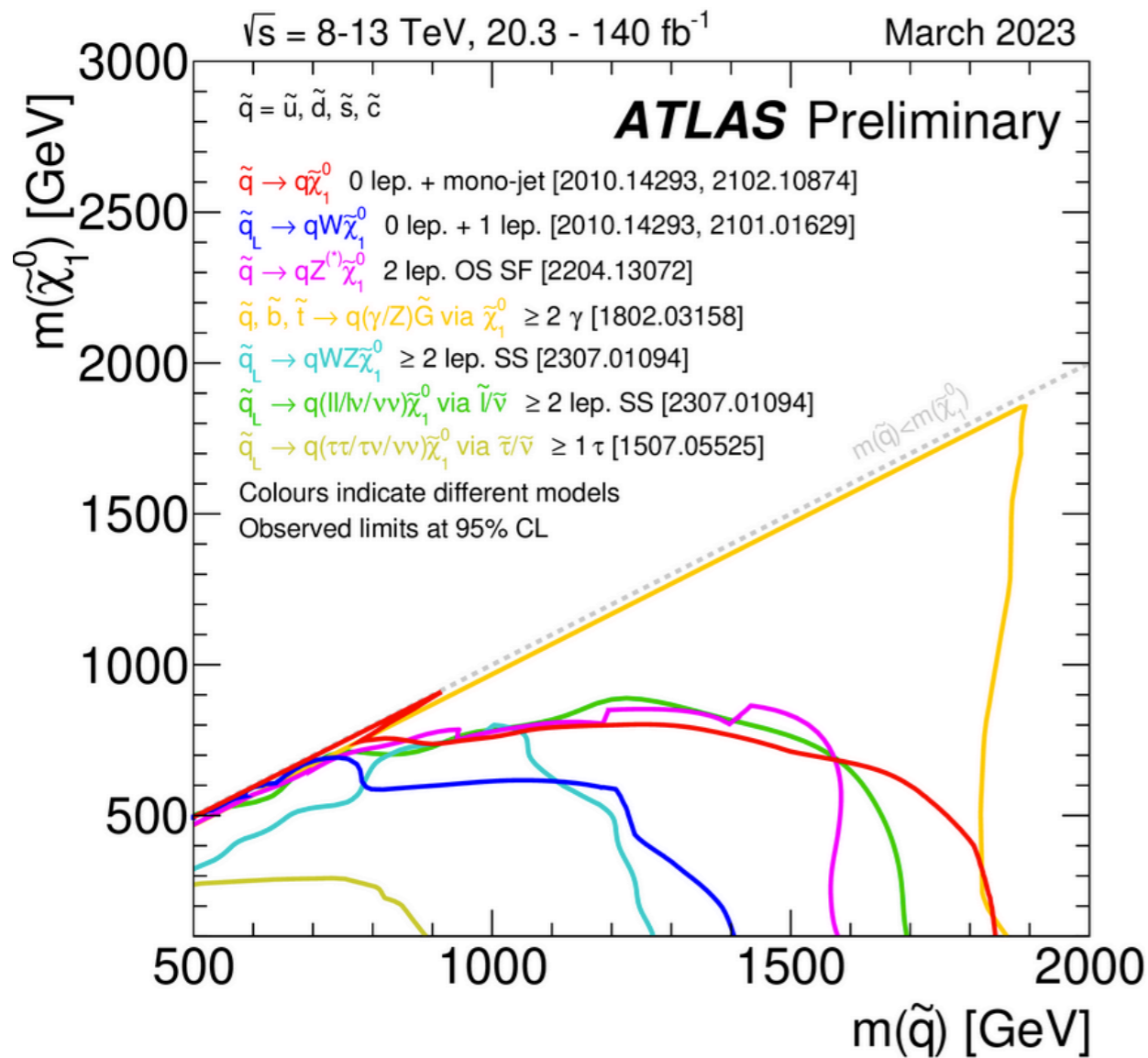
The SUSY production @ 13TeV

Strong SUSY: larger cross-section; energetic jet activity.



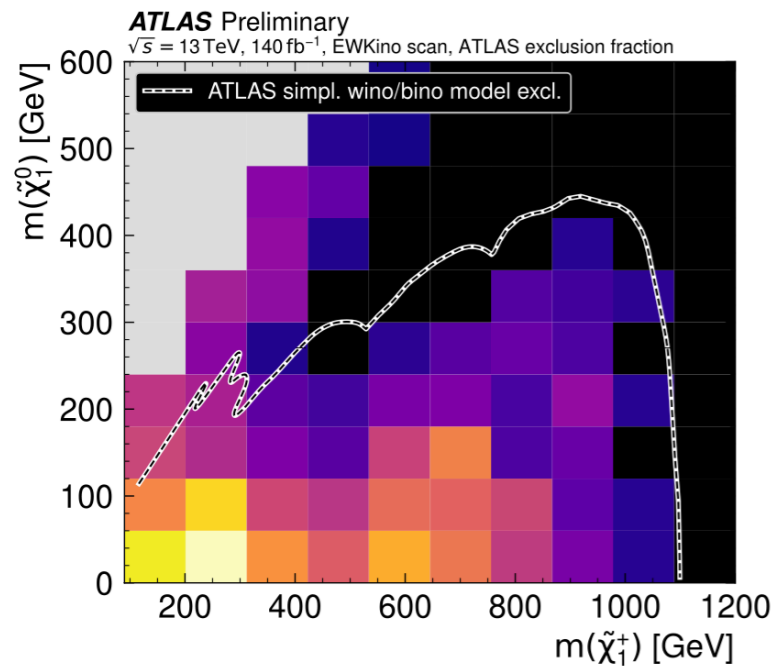
Electroweak SUSY: smaller cross-section; less jet; cleaner signature.

Squark summary



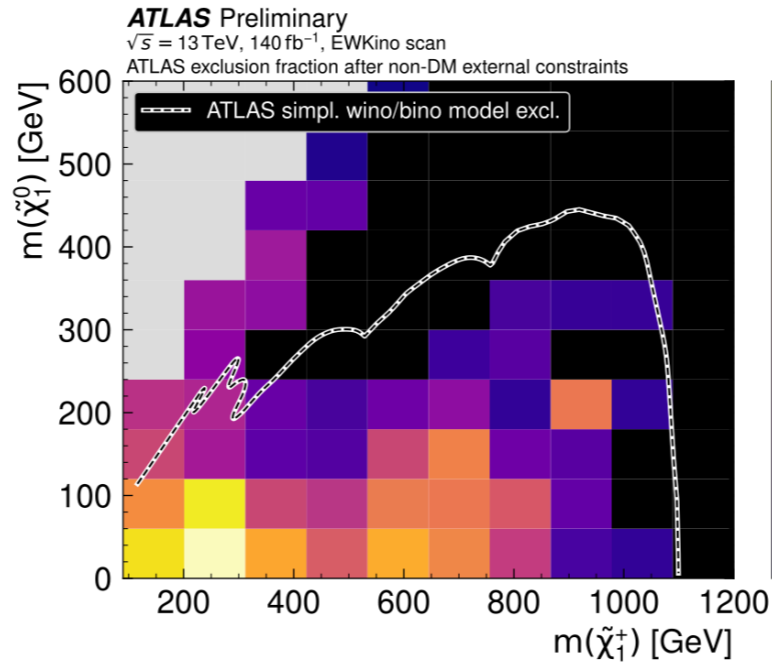
pMSSM

- The fraction of models excluded by the ATLAS Run 2 electroweak searches
- Plots are overlaid with a contour indicating the exclusion for relevant simplified models



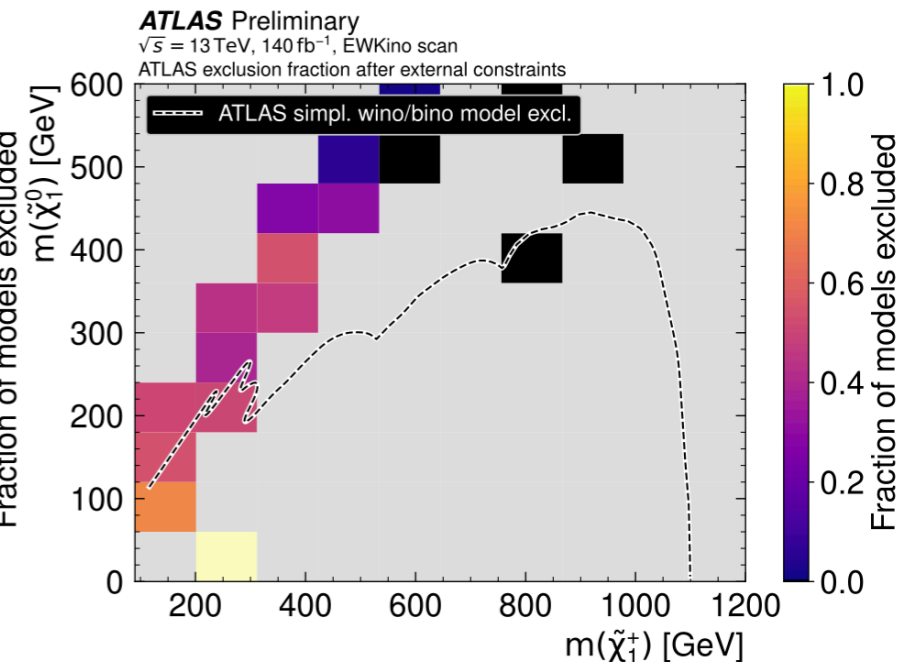
(a) All models

No external constraints



(c) Models passing non-DM external constraints

flavour, precision EWK constraints

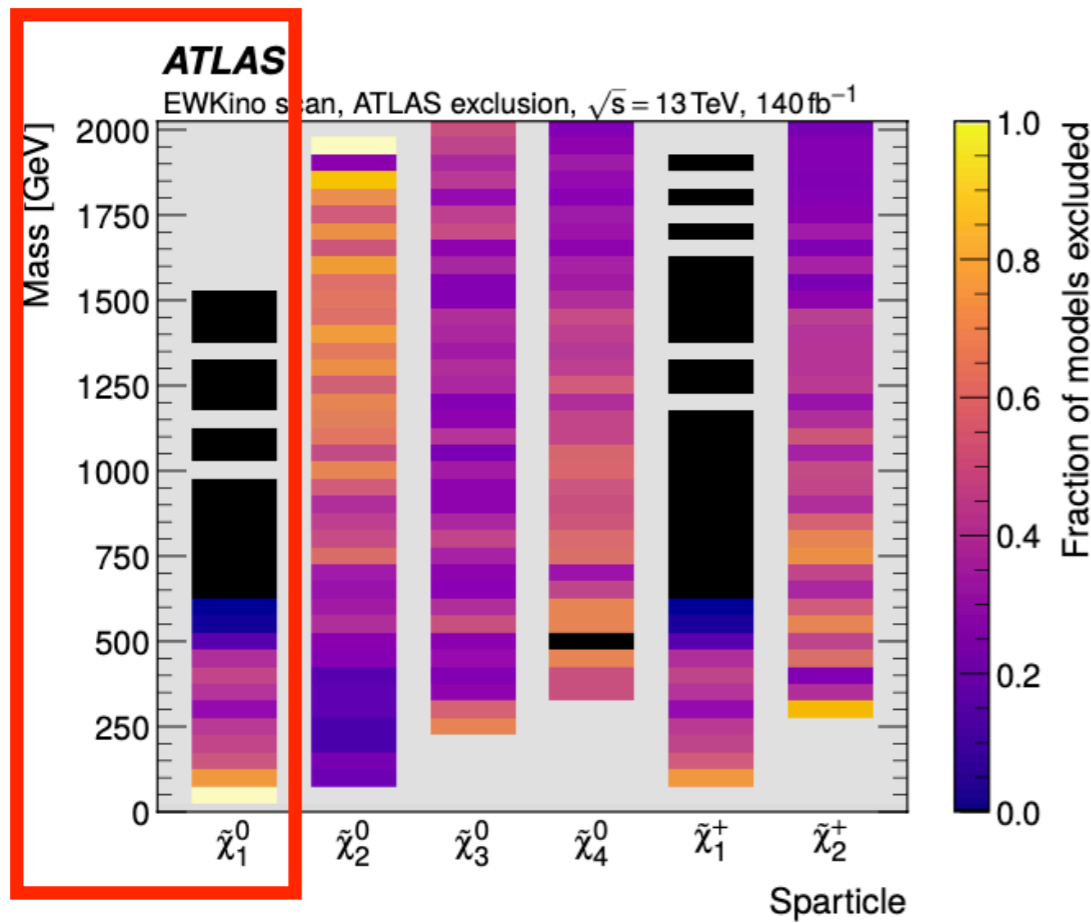


(e) Models passing all external constraints

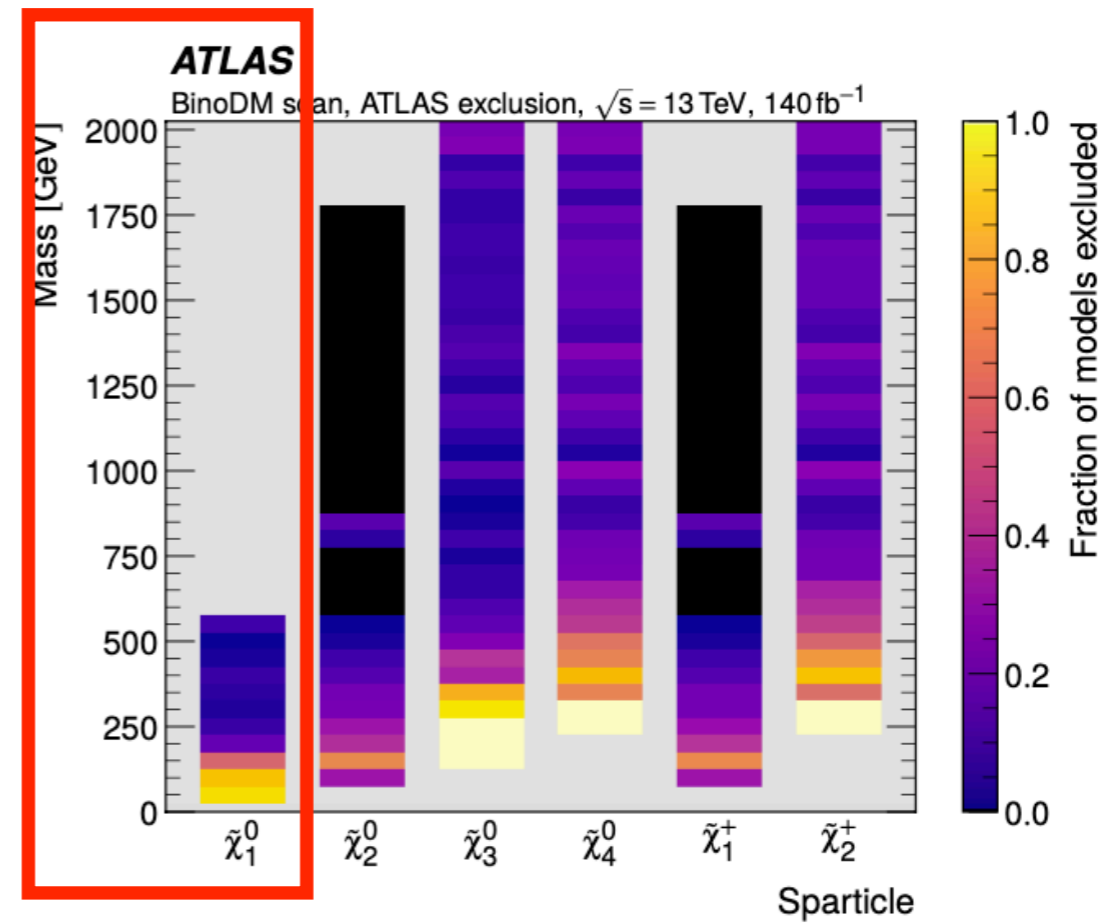
flavour, precision EWK & DM constraints

- Most of the excluded models are inside the simplified model contour
- Although most inside contour models can be removed by the external constraints due to the DM relic density requirement which suppresses bino-LSP models
- A majority of the remaining models lying in the diagonal with small mass splittings

Fraction of models excluded by ATLAS for models satisfying all of the external constraints



(a) EWKino scan



(b) BinoDM scan

The fraction of models excluded decreases with increasing LSP mass.